DEVELOPMENT OF AN IMPROVED ANALYTICAL TECHNIQUE FOR LEAD DETERMINATION, AND ITS APPLICATION TO STUDIES IN LEAD CONTENT IN SEAFLOOR HYDROTHERMAL CHIMNEYS FROM GUAYMAS BASIN, GULF OF CALIFORNIA; PACMANUS, EASTERN MANUS BASIN; AND THE SOUTHERN EAST PACIFIC RISE

by

Cheyenne Loon

A thesis submitted in conformity with the requirements
for the degree of Master of Science
Graduate Department of Geology
University of Toronto

DEVELOPMENT OF AN IMPROVED ANALYTICAL TECHNIQUE FOR LEAD DETERMINATION, AND ITS APPLICATION TO STUDIES IN LEAD CONTENT IN SEAFLOOR HYDROTHERMAL CHIMNEYS FROM GUAYMAS BASIN, GULF OF CALIFORNIA; PACMANUS, EASTERN MANUS BASIN; AND THE SOUTHERN EAST PACIFIC RISE

Cheyenne Loon, Graduate Department of Geology, University of Toronto
Master of Science Degree, 1999

Abstract

Analysis by solution methods of Pb in seafloor sulfides has been unreliable due to incomplete dissolution, frustrating attempts to understand the geochemistry of Pb in seafloor hydrothermal systems. Bulk Pb recoveries were improved by fully digesting samples prior to analysis by ICP-AES. Following decomposition by HNO_3-HF-$HClO_4$, insoluble $(Pb,Ba)SO_4$ residues were digested in microwave-heated $Na_2CO_{3(aq)}$. Lead recoveries averaged 88% from an in-house standard and 91%-98% from CANMET ore standards. Recovery was influenced by variations in $[HNO_3]$ and $Na_2CO_{3(aq)}$ temperature.

Chimneys from three vent sites - PACMANUS, Guaymas Basin, and Pito Deep - were analysed for Pb, resulting in concentrations of 0.005-1.3 wt.% (PACMANUS) and 0.009-0.4 wt.% (Guaymas Basin). Sulfides from Pito Deep yielded a mean result of 0.06 wt.% (n=2). Pb in felsic volcanics from the Pacific Antarctic Rise was in the range <0.006 - 1.2 ppm.

Pb correlates with Na, Cd, As, Sb, Ag, and Zn in PACMANUS chimneys (95% confidence). Correlation with these elements in Guaymas Basin samples was not significant.

ACKNOWLEDGMENTS

It was Professor Steve Scott's infectious enthusiasm for the study of seafloor hydrothermal systems that first drew me to the field as a second-year undergraduate. Those first few months as his research assistant paved the way and inspired me to return for further study as a graduate student. Over the course of this project, the guidance of Professors Steve Scott and committee members Mike Gorton and Ed Spooner was indispensable. Their many suggestions, and their patience when the going got tough, is very much appreciated.

The experimental portion of this thesis would have not been possible without Professors Don Chipley, Mike Gorton, and Ron Barefoot, as well as Andrew Wolf and Neil Arner - they were generous with lending equipment as I set up my lab; and they were generous with their advice. Jan Peter and Roger Hékinian provided the samples from Guaymas Basin and southern East Pacific Rise, respectively. John Rucklidge and Claudio Cermignani guided my efforts on the electron microprobe. Pamela Wee (Perkin-Elmer) kindly lent her expertise to the interpretation of the ICP-AES data. And Roger Moss was always ready with advice on the finer points of working with seafloor rocks.

My family has been a great source of support and understanding over the course of this project, for which I am grateful. I'd also like to thank my fellow SMGRL labmates and my officemates for their friendship and encouragement.

Research for this study was financially supported by grants from NSERC and the Bank of Nova Scotia, held by Professor Scott. The author was financially supported by a generous grant from the Cree School Board Postsecondary Program and a University of Toronto Open Fellowship.

TABLE OF CONTENTS

LIST OF FIGURES

LIST OF TABLES

LIST OF APPENDICES

CHAPTER 1:

DEVELOPMENT OF AN IMPROVED ANALTICAL TECHNIQUE FOR LEAD DETERMINATION OF SEAFLOOR HYDROTHERMAL CHIMNEYS

INTRODUCTION

Bulk lead determinations in seafloor geological material are performed by inductively coupled plasma atomic emission spectrometry and mass spectrometry (ICP-AES, ICP-MS), atomic absorption spectrometry (AAS), and X-ray fluorescence (XRF). Determination by AAS and ICP methods, both requiring lead being in solution, is thought to be generally interference-free, whereas Pb peaks in XRF spectra are subject to severe interferences by Ba (Binns et al. 1993).

The dissolution of samples, in preparation for analysis by ICP-MS, ICP-AES or AAS, comes with its own potential pitfalls. Incomplete dissolution, resulting in insoluble residues after acid attack, is particularly common in geological material (Boss and Fredeen, 1989). Barite, with a solubility of 0.000222 g/100cc (Weast, 1969), is impervious to acid attack. The formation of other insoluble precipitates after acid attack of sulfides is well-documented (e.g., Smith and Cousins, 1985; Lamothe et al. 1986). The oxidation of metal sulfides by HNO_3 yields $SO_4^{2-}{}_{(aq)}$, which subsequently combines with cations to precipitate sulfates. Lead is particularly vulnerable to this effect. ICP determinations of lead-rich ores and sulfides commonly results in reduced lead recoveries due to the precipitation of $PbSO_4$ (Lamothe et al., 1986; L. Dotter, CSIRO, personal communication, 1997). The substitution of HCl for HNO_3 does not solve the problem because it results in the precipitation of PbCl and other chlorides.

This problem is particularly relevant to the study of modern seafloor hydrothermal chimneys, whose barite contents range from trace amounts at mid-oceanic ridges (Scott, 1997) up 30% by volume at seamounts (Hannington, 1986) and back-arc settings (Scott, 1997). Anglesite ($PbSO_4$), a minor phase present in chimneys from the PACMANUS deposit (J. Parr, CSIRO, personal communication, 1997), the Jade deposit, 13°N EPR (as summarised by Scott, 1997), and at Conical Seamount (Herzig et al. 1996), is also highly insoluble in acid (solubility 0.00425 g/100 cc). Consequently, bulk Pb determinations of seafloor sulfide materials by ICP or AAS methods require the inclusion of a digestion scheme able to decompose barite, anglesite, and precipitated lead sulfate completely.

Preliminary examinations of partially digested chimney material included in this study supported this assertion. Insoluble white material, recovered from trial HNO_3-HF-$HClO_4$ digestions of barite-rich chimneys, was analysed for Pb by XRF. Concentrations of up to 1 % (wt.) Pb were detected, which could not be further quantified due to the effects of severe barium interference and low sample weight (approximately 100 mg). Subsequent examination by scanning electron microscopy (SEM) failed to locate individual particles of $PbSO_4$. Assuming total lead occurs as $PbSO_4$, the proportion of 1.5 mg $PbSO_4$ per 100 mg barite suggests this search is of the "needle in a haystack" variety, frustrating any effort to quantify Pb loss by examination of insoluble residues.

Non-fusion methods of sulfate dissolution, while not unknown in the literature (see below), are not in wide use for ICP determinations of geological materials. Furnace-heated Na_2CO_3 solutions are effective, but heating times of up to 1.5 days (Parisot, 1997) add considerably to sample preparation times. Microwave-assisted digestion, first introduced in the mid-1970's (King and Barclay 1997), is a vehicle to rapid, even automated, decomposition of

geological materials. This study introduces the use of a microwave oven to sulfate digestion by aqueous Na_2CO_3, in the interests of shortening sample preparation times.

Previous work

The HNO_3-HF-$HClO_4$ mixed acid digestion of geological materials is in common use as a method for sample digestion in preparation for analysis by ICP-AES, ICP-MS, or AAS (e.g., Ontario Geological Survey, 1990; Chao and Sanzolone, 1992; Totland et al., 1992). Though designed to decompose a wide range of minerals and other compounds, this acid combination is nevertheless ineffective against certain notable acid-resistant minerals and precipitates.

The complete dissolution of barite and other refractory sulfates has long been problematic. Although fusion with lithium metaborate or Na_2CO_3 is effective, the procedure is time-consuming (Puchelt and Setiobudi, 1989), and, in the case of carbonate fusions, can result in incomplete digestion of barite (Sen Gupta, 1991). Fusion by lithium metaborate has been known to reprecipitate barite (Sen Gupta, 1991). Totland et al. (1992) reported volatile losses for elements including lead in standard geological reference materials treated with a $LiBO_2$ fusion.

Several newer methods of sulfate decomposition have been developed for the purpose of elemental analysis by AAS or ICP. For example, Puchelt and Setiobudi (1989) successfully dissolved barite, celestite, anglesite and anhydrite in a heated hydroxylamine-hydrochloride - nitric acid solution. However, these solutions remained stable for only 8 hours (Puchelt and Setiobudi, 1989), rendering their results nonreproducible. Barite was also found to be dissolvable in a boiling disodium-EDTA-ammonium hydroxide solution (Sen Gupta, 1987 and

1991), but this method is limited by its ineffectiveness in attacking other refractory sulfates including $PbSO_4$ (J.G. Sen Gupta, personal communication, 1997).

Leaching $PbSO_4$ with aqueous Na_2CO_3 is a process frequently employed in the metallurgical industry in the recovery of lead from spent storage batteries (Chen and Dutrizac, 1996). In the presence of aqueous Na_2CO_3, $PbSO_4$ is converted to the acid-soluble lead carbonate compounds $Pb_3(CO_3)_2(OH)_2$ (hydrocerussite) and $NaPb_2(CO_3)_2(OH)$. Mild reaction conditions (dilute 0.1 M Na_2CO_3) favour the formation of hydrocerussite. At higher Na_2CO_3 concentrations (1.0 or 2.0 M) or higher temperatures, $NaPb_2(CO_3)_2(OH)$ forms.

Castillejos et al. (1996) showed that celestite ($SrSO_4$) also reacts to form Sr carbonate in the presence of heated aqueous Na_2CO_3. The conversion of $(Pb,Ba,Sr)SO_4$ to carbonate is thought to obey a shrinking core model (Gong et al., 1992a and Castillejos et al., 1996), where CO_3^{2-} ions diffuse through a porous 'product layer' composed of hydrocerrusite (in the case of Pb) surrounding each particle.

Geological studies using closed-vessel digestions with 1:10 (Breit, Simmons and Goldhaber, 1985) and 1:20 (Parisot, 1997) Na_2CO_3 solutions achieved complete decomposition of barite for the purposes of $^{87}Sr/^{86}Sr$ and lead isotopic analyses, respectively. Digestions were carried out in a furnace, with reaction times varying between 4 hours (Breit, Simmons and Goldhaber,1985) and 1.5 days (Parisot, 1997), depending on the Na_2CO_3 solution concentration. Although this procedure has been shown to be effective in the recovery of Pb or Sr cations from the barite matrix for isotopic determinations, it has apparently not been employed for dissolution of $PbSO_4$ in geological materials, either as the mineral anglesite or as a chemical precipitate produced during HNO_3 oxidation of Pb-rich sulfides.

Previous work shows that closed-vessel digestions are preferable to open-vessel (i.e. not sealed) procedures. High recoveries for trace elements including Pb have been reported for closed-vessel acid digestions (Lamothe et al., 1986; Totland et al., 1992; Nakashima et al., 1988; Mahan et al., 1987). Lead losses of up to 20% (Nakdarni 1984) through volatilisation have been recorded in several types of microwave-assisted open-vessel acid digestions (Totland et al. 1992).

ANALYTICAL METHOD

Instrumentation

The Perkin-Elmer 4000 Atomic Absorption Spectrophotometer, with an air acetylene flame, was used for preliminary bulk Pb determinations. Subsequent multi-element analyses were carried out using a Perkin-Elmer Optima 3000DV ICP-AES, equipped with an autosampler. Instrument operating parameters are summarised in Table 1.1. The accompanying Perkin-Elmer ICP WinLab software package, version 1.40, was used to process raw data.

A domestic "kitchen" type General Electric (Model GTC1042W J01) microwave oven, equipped with a rotating stage, was used for Na_2CO_3 digestions. Variable power output settings allowed power increases in increments of 10%, with a maximum power output of 625 W.

Standards

Two CCRMP CANMET certified ore standards - MP-1a (Mount Pleasant) and KC-1 (Kidd Creek) - were analysed to test lead recoveries. Also included were two in-house synthetic rock standards - PAC and GUA - created to mimic typical chimney compositions from PACMANUS and Guaymas Basin, respectively. This was accomplished by combining varying proportions of reagent SiO_2, $CaCO_3$, and $BaSO_4$ with MP-1a standard. Descriptions and compositions of all standards are outlined in Tables 1.2, 1.3a and 1.3b.

Procedure

The microwave unit was calibrated in accordance with EPA (U.S. Environmental Protection Agency) Method 3051 (Appendix 1). A linear relationship between the strength of the microwave

TABLE 1.1: Operating parameters for ICP-AES

Instrument	Perkin-Elmer Optima 3000DV ICP-AES	
Plasma RF power	1300 W	
Plasma flow	15 L/min	
Auxiliary gas flow	0.5 L/min	
Nebuliser gas flow	0.8 L/min	
Sample uptake rate	1 ml/min	
Sample delay	10s	
Washing time	up to 30s	
Resolution	normal	
View mode	Axial	
	ICP run 1	*ICP run 2*
Maximum read time	5s	10s
Minimum read time	1s	2s

TABLE 1.2: Description of Standards Used in this Study

Standard	Type	Description
KC-1	CANMET-CCRMP Reference Ore	Kidd Creek Zn-Pb-Sn-Ag ore
MP-1a	CANMET-CCRMP Reference Ore	Mt. Pleasant Zn-Sn-Cu-Pb ore
PAC	In-house	synthetic PACMANUS chimney
GUA	In-house	synthetic Guaymas Basin chimney

TABLE 1.3a: Compostion of CANMET Standards

Standard	Element	Concentration (wt. %)
KC-1	Zn	20.07
	Pb	6.87
	Sn	0.67
	Cu	0.112
	Ag	0.112
MP-1a	Zn	19.02
	Pb	4.33
	Cu	1.44
	Sn	1.28
	As	0.84
	In	0.033
	Bi	0.032
	Mo	0.029
	Ag	69 μg/g

TABLE 1.3b: Compostion of Synthetic In-House Standards

Standard	Component (reagent)	Fraction (wt. %)	Element	Concentration (wt. %)
PAC	$BaSO_4$	30.00	Ba	17.66
	SiO_2	10.00	Si	0.046
	MP-1a	60.00	Zn	11.412
			Pb	2.598
			Cu	0.864
			Sn	0.768
			As	0.504
GUA	$BaSO_4$	9.00	Ba	5.29
	SiO_2	20.00	Si	0.093
	$CaCO_3$	70.00	Ca	28.03
	MP-1a	1.00	Zn	0.1902
			Pb	0.0433
			Cu	0.0144
			Sn	0.0128
			As	0.0084

field (in watts) and the manufacturer's power settings was established (Figure 1.1). As described by Kingston (1997), this calibration is recommended in the documentation of a heating routine in microwave units not equipped with temperature feedback control. Thus the reaction conditions (i.e., the microwave field) can be closely reproduced, provided the loading (i.e., digestion vessels) in the unit is the same.

For digestion (see Figure 1.2 and Appendix 2 for details), approximately 0.5g of powdered rock sample was placed in a 60 ml Teflon vessel. Sulfides, carbonates and organic matter were digested with concentrated HNO_3, followed by evaporation to incipient dryness. Concentrated HF-$HClO_4$ was added to digest oxides, silicates and chlorides. After the removal of HF and $HClO_4$ by evaporation, residues were taken up in dilute HNO_3 and set aside for dilution and analysis by ICP-AES. Chemical constants for all reagents used in the acid digestion procedure are listed in Appendix 3.

All remaining undissolved solids were returned to the Teflon vessel. After the addition of Na_2CO_3 solution, the vessels were capped and heated in a microwave oven. The heating routine (Table 1.4), repeated once, was as follows - 3 minutes at 190 W (30% power), 3 minutes at 625 W (100% power), 10 minutes at 190 W (30% power), 5 minutes in an ultrasonic bath. The resulting solids were filtered, rinsed, and dissolved in dilute HNO_3.

Two component solutions were analysed for each rock sample. Solutions resulting from the HNO_3-HF- $HClO_4$ acid digestion step were labelled 'b' solutions. Solutions from the microwave-assisted Na_2CO_3 digestion were labelled 'g' solutions. These solutions were kept separate to prevent sulfate reprecipitation. The 'b' solutions were diluted to volume in a 100 ml volumetric flask, and 'g' solutions were diluted to 25 ml. All diluted solutions had a final acidity

Figure 1.1: Linear calibration for absorbed power from a domestic microwave oven, Sanyo Model EM-256WS

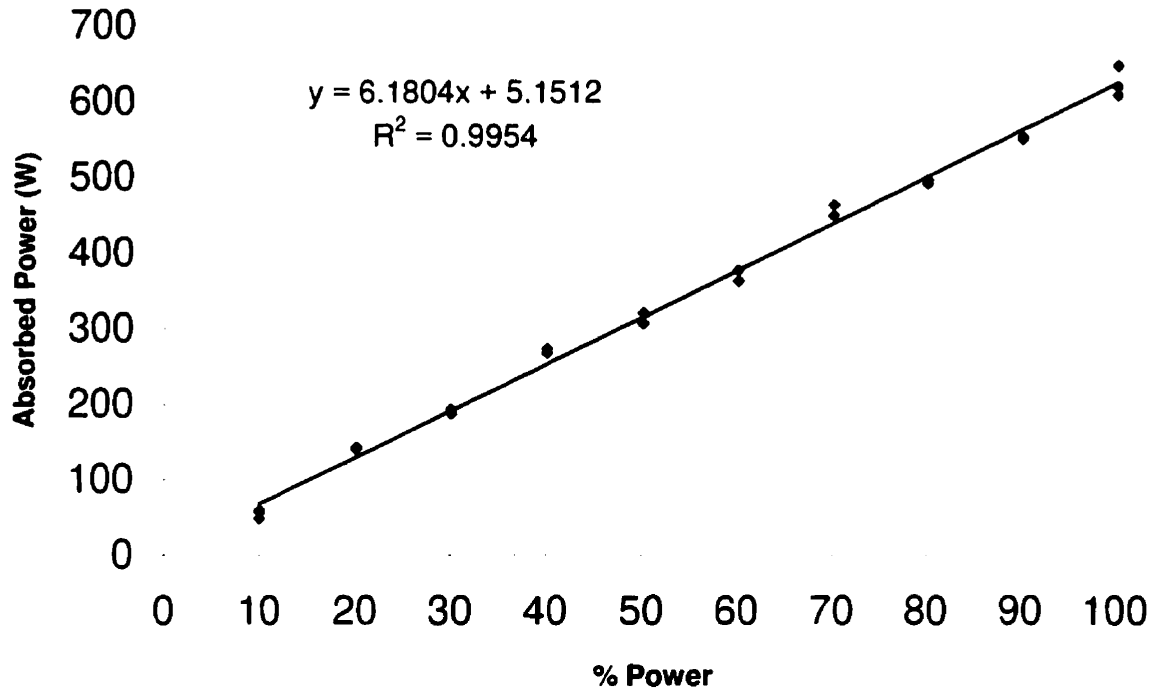

Figure 1.2: Flowsheet for sample digestion

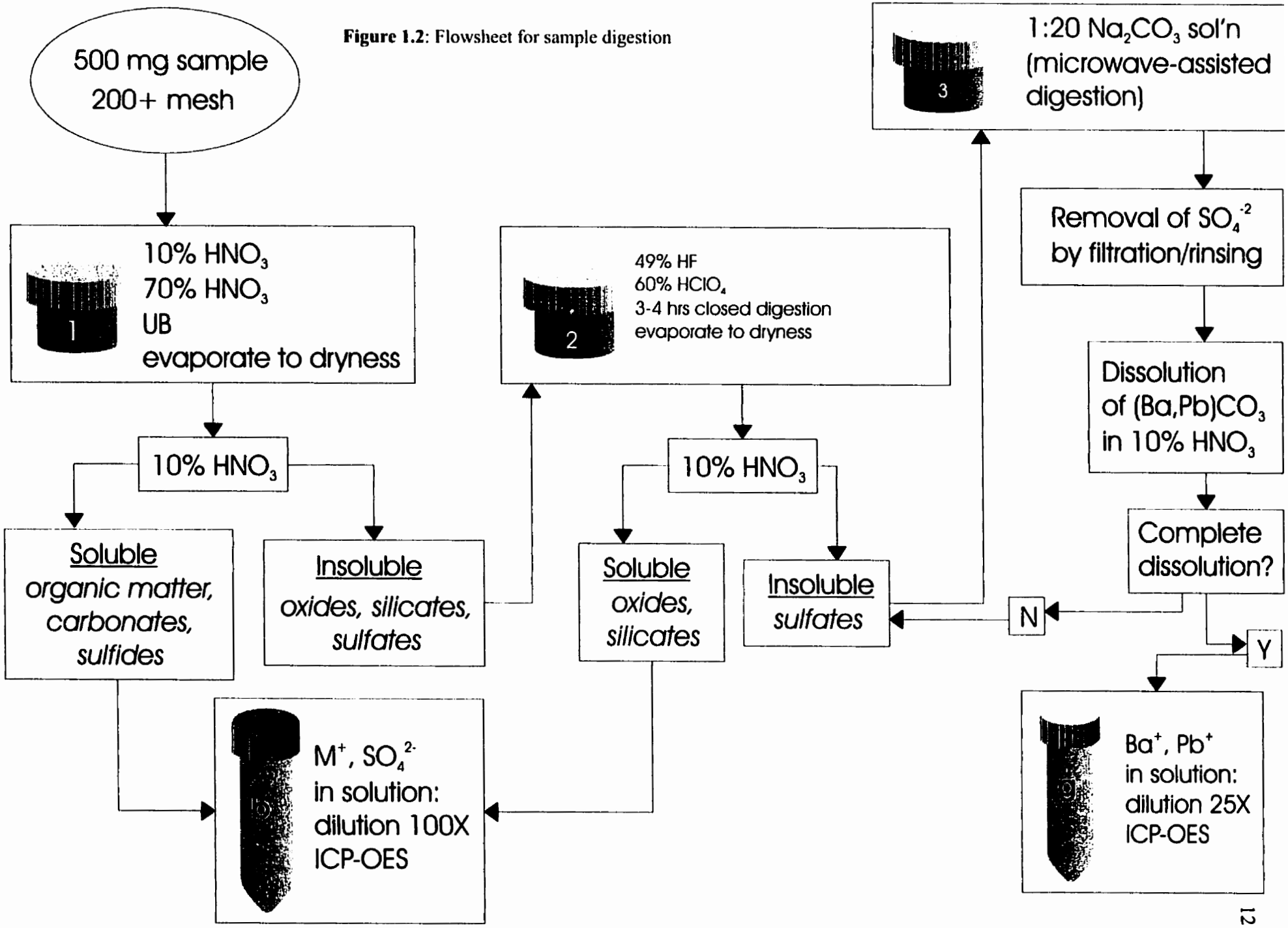

TABLE 1.4: Microwave heating routine

Time (minutes)	Power Setting (%)	Power Output (W)
3	30	191
3	100	623
10	30	191
5[1]	0	0
3	30	191
3	100	623
10	30	191
5[1]	0	0

[1] 5 minutes in ultrasonic bath

TABLE 1.5: List of multielement ICP standards

Standard	Concentration (ppm)	Elements
s1-0.1	0.1	Mg, Si, K, Ca, Fe
s1-100	100	
s2-0.1	0.1	Na, K, Mn, Fe, Co, Ni, Co, Zn, Cd, Hg, Pb
s2-100	100	
s3-0.05	0.05	Na, Mg, Al, Si, K, Ca, Mn, Fe, Co, Ni, Cu, Zn, Sr, Cd, Hg, Pb
s3-0.5	0.5	
s3-5	5	
s3-50	50	
s4-0.05	0.05	As, Sn, Sb, Ba, La
s4-0.5	0.5	
s4-5	5	
s4-50	50	

Multi-element standards s1 and s2 diluted to concentrations of 0.1 and 100 ppm.
Multi-element standards s3 and s4 diluted to concentrations of 0.05, 0.5, 5 and 50 ppm

of 2% HNO_3. Multi-element ICP standards were prepared at concentrations of 0.05, 0.5, 5.0 and 50 ppm in 2% HNO_3 (Table 1.5).

Appendix 4 lists the theoretical reactions describing the digestion of Pb sulfide and $PbSO_4$. Appendix 5 details the procedure and results of preliminary experiments confirming that $(Pb,Ba)SO_4$ quickly converts to carbonate in the presence of microwave-heated aqueous Na_2CO_3.

All the rock samples were digested in one of five separate batches. All resulting solutions were analysed over two ICP runs, conducted on separate dates (Table 1.6).

TABLE 1.6: Digestion batches and analytical runs

SAMPLE DIGESTION		ICP-AES ANALYSES	
		Samples	
Batch number	**Comments**	**Run 1**	**Run 2**
1	· concentrated HNO_3 · sulfates separated by centrifuge and decanting TLL[a] = 130 ml	· PACMANUS 118693 subsamples · all Guaymas subsamples	
2	· sulfates separated by centrifuge and decanting TL = 130 ml	· PACMANUS 132452, 132744; and 118693 replicates · selected Guaymas replicates	
3	· sulfates separated by centrifuge and decanting TLL = 277 ml	· PACMANUS 118693 replicates · selected Guaymas replicates	
4	· sulfates separated by filtration TLL = 155 ml		· PACMANUS 118693 replicates · selected Guaymas replicates · GUA · MP-1a
5	· sulfates separated by filtration TLL = 250		· PACMANUS 118693 replicates · selected Guaymas replicates · all s-EPR samples · KC-1 · replicates for GUA, PAC, MP-1a

[a]TLL (total liquid load) refers to sum volume of $Na_2CO_{3(aq)}$ in all vessels, present in the microwave oven during heating.

RESULTS

All standards and samples were background corrected by subtracting an HNO_3 blank from all peaks. Calibration of the signal intensity was based on the ICP multi-element standards s3 and s4, diluted to concentrations of 50, 5, 0.5 and 0.05 ppm (Table 1.5). Signal intensities (counts per second) were converted to ppm with a two-point calibration line based on the 5 ppm standards (s3-5, s4-5) and the zero intercept. Multi-element standards s1 and s2, at dilutions of 0.01 and 100 ppm, provided a check on the linear dynamic range (LDR). Standards s3-5, s4-5, s3-50 and s4-50 were also run as samples for quality control.

The instrument was set to read signal intensities in axial view. This resulted in improved sensitivity at lower concentrations at the expense of the better linear dynamic range (LDR) found in radial view. Diminished signal intensities in the quality control standards s3-50, s4-50, s1-100, and s2-100 were attributed to instrumental error due to inefficient aspiration in the Nebuliser. Samples with Pb concentrations in the upper range (40 to100+ ppm) were recalibrated and scaled up using the 50 and 100 ppm standards.

The background signal was calculated as an average of a total of nine measurements from three 2% HNO_3 blanks. The detection limit for Pb, calculated as $3\sigma_{background}$, was 0.006 μg/ml, based on its spectral line at 220.353 nm.

The lower limit of the linear dynamic range (LDR) is calculated as 5 × detection limit. Boss and Fredeen (1989) reported a typical ICP-AES detection limit for Pb to be 40 μg/L (0.04 μg/ml) in radial mode, which translates to 0.004 μg/ml for axial mode. The upper limit of the

LDR is generally cited to be 100 μg/ml for Pb, but may be as high as 200 μg/ml (P. Wee, Perkin-Elmer, personal communication, 1998).

For this study, the lower limit for the LDR is estimated to be 5 × 0.006 μg/ml = 0.03 μg/ml. The upper limit was severely diminished due to probable instrument error, resulting in a LDR of roughly 0.03 μg/ml to <50 μg/ml. However, accuracies for Pb dilutions to 0.01 μg/ml were within acceptable limits and all data greater than 2 × detection limit was accepted.

Lead concentrations in ppm, or μg/g, was calculated as follows:

$$\frac{(\mu g\ Pb \text{ in 'b'solution}) + (\mu g\ Pb \text{ in 'g'solution})}{g \text{ total sample weight}}$$

After acid and Na_2CO_3 digestion, standards yielded mean Pb values ranging from 75% to 98% of the expected value (accuracy within -1.88% to -25.88%), depending on the standard (Table 1.7).

Mean values for Mg, Ca, Fe, Cu, Pb, As, and Sn are summarised in Table 1.8. Recoveries and relative precisions for Na, Mg, K, Ca, Mn, Fe, Co, Ni, Cu, Sr, Cd, Hg, Pb, As, and Sn are summarised in Table 1.7.

Poor recoveries for Sn (<15%) in MP-1a and KC-1 are due to the refractory nature of cassiterite (Lamothe et al., 1986), the main tin-bearing phase in both CANMET standards (Steger and Bowman, 1982 and Faye et al., 1974). Unusually high Mg in GUA may be due to contamination from $CaCO_3$ added in the preparation of GUA.

Table 1.7 : Relative precision and recoveries for elements determined by ICP-AES

	PAC		GUA		MP-1a		KC-1
	relative precision	% recovery	relative precision	% recovery	relative precision	% recovery	% recovery[a]
Na	1.7		2.4		1.1		
Mg	9.3	93	32.2	3170[b]	17.0	97	
K	0.8		1.6		0.7		
Ca	1.9	91	2.4	70	2.5	89	
Mn	0.9		7.3		0.9		
Fe	0.8	87	3.2	86	1.2	92	
Co	15.6				3.7		
Ni	5.3		28.7		32.0		
Cu	1.3	106	7.4	102	1.2	99	104
Sr	7.0		7.7		161.7		
Cd	1.4		3.1		0.5		
Hg	11.0		14.5		11.2		
Pb	6.3	88	3.5	75	1.0	98	91
As	2.1	84	3.6	77	0.9	86	
Sn	38.2	9			1.2	13	1

[a]n=1 for KC-1; no precision data available

[b]high Mg due to contamination from the $CaCO_3$ component of GUA

Table 1.8: ICP-AES results for certified and information values from in-house and CANMET standards

	PAC (n = 3)		GUA (n = 4)		MP-1a (n = 3)		KC-1 (n = 1)	
	R	M	R	M	R	M	R	M
Mg	0.012	0.011 ± 0.001	0.0002	0.0063 ± 0.002	0.02	0.019 ± 0.003		0.039
Ca	0.900	0.821 ± 0.016	28.0150	19.6229 ± 0.465	1.50	1.33 ± 0.03		0.22
Fe	3.720	3.228 ± 0.026	0.0620	0.0531 ± 0.002	6.20	5.71 ± 0.07		11.17
Cu	0.864 ± 0.006	0.915 ± 0.012	0.0144 ± 0.0001	0.0147 ± 0.0011	**1.44 ± 0.01**	1.535 ± 0.018	**0.112 ± 0.005**	0.117
Pb	2.598 ± 0.018	2.274 ± 0.144	0.0433 ± 0.0003	0.0324 ± 0.0011	**4.33 ± 0.03**	4.248 ± 0.041	**6.870 ± 0.10**	6.276
As	0.504 ± 0.012	0.424 ± 0.009	0.0084 ± 0.0002	0.0065 ± 0.0002	**0.84 ± 0.02**	0.72 ± 0.01		
Sn	0.768 ± 0.024	0.076 ± 0.028	0.0128 ± 0.04	b/d	**1.28 ± 0.04**	0.167 ± 0.002	**0.67 ± 0.04**	0.0045

All values in %

R recommended value

M measured value

b/d below detection limit

Bold numbers signify certified values for CANMET standards MP-1a and KC-1

Mg, Ca, Fe are information values for MP-1a (CANMET Report 82-14E); no precision given

Si data was omitted because the majority of Si was volatilised as silicon tetrafluoride, SiF_4 (Totland et al.,1992), during HF-$HClO_4$ digestion. Precious metal determinations by ICP-AES proved inconclusive because dilutions optimal for Pb determination (0.5 - 100 μg/ml) fell below detection limits for gold and silver. Conversely, signal intensities for Ca, Ba, Fe and Zn in many cases exceeded their 100 μg/ml upper linear calibration range. Complete signal saturation of all three Ca lines was observed in several Guaymas subsamples.

Three s3 standard solutions were spiked with an ICP calcium standard to test the effect of a high Ca load on Pb detection (Figure 1.3). The resulting solutions -- s3-0.05-ca, s3-0.5-ca and s3-5-ca -- each contained 990 ppm Ca. After background corrections, ICP results showed a 20% peak increase in all three Ca-spiked solutions when compared with the unspiked s3 standards. This effect was observed for all elements in s3, including Ni, Co, Fe, Cu, Pb, Mn and Hg. Two replicate s3-5 standard solutions spaced in the middle and end of the run verified minimal instrument drift.

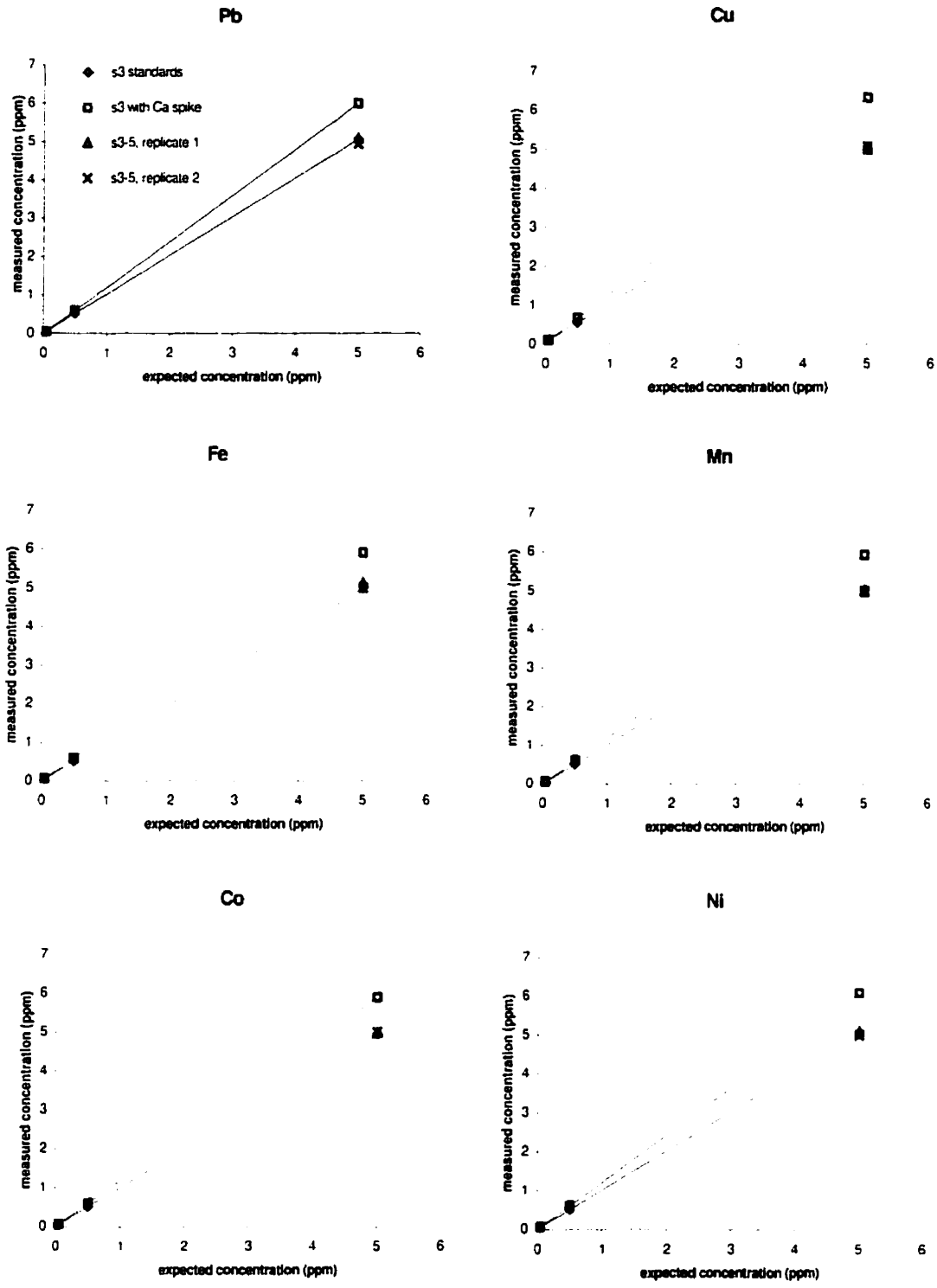

Figure 1.3: Effect of 900 ppm Ca spike on selected elements in multielement standards s3-0.05, s3-0.5 and s3-5. A 20% enhancement is observed in Pb, Cu, Fe, Mn, Co and Ni. Replicates of s3-5 show minimal instrument signal drift.

DISCUSSION

Recoveries from the standards are represented in log-log plots comparing expected and measured values for selected elements (Figure 1.4). Log-log plots, described in further detail by Totland et al. (1992), compare element recoveries at different concentrations, and are useful in evaluating the overall effectiveness of the digestion procedure with respect to varying standard preparations.

A linear regression with a slope = 1 suggests a digestion of maximum efficiency. Log-log plots for MP-1a, PAC and GUA show that Pb results agree with overall recoveries for each standard. Low lead recovery in GUA (75%) corresponds with an overall slope of 0.7004; improved lead recoveries in PAC (88%) and MP-1a (99%) are reflected in increased slopes respectively (PAC = 0.8778; MP1a = 0.9418).

The systemic low recoveries of all metals derived from the MP-1a fraction of GUA prompted a closer re-examination of the digestion procedure. In all GUA replicates (n = 4), it was found that, after the HNO_3-HF-$HClO_4$ step, non-acid-digested residues consistently weighed less than 9%, the expected $BaSO_4$ fraction, of the total weight (Table 1.9). It was concluded that during preparation of the GUA in-house standard, less $BaSO_4$ and MP-1a was added than stated. The error could not be corrected for, since the proportions of $BaSO_4$, $PbSO_4$, and SnO_2 in the 'g' residues was not quantifiable. The GUA results were nevertheless included, because they supplement the data set used to study the behaviour of Pb during the Na_2CO_3 digestion.

Post-Na_2CO_3 digestion Na^+, SO_4^{2-} -rich solutions from four samples were analysed by ICP-AES to check if an incomplete conversion of $PbSO_4$ to carbonate may have 'leaked' Pb^{++} to the solution. No significant Pb was found.

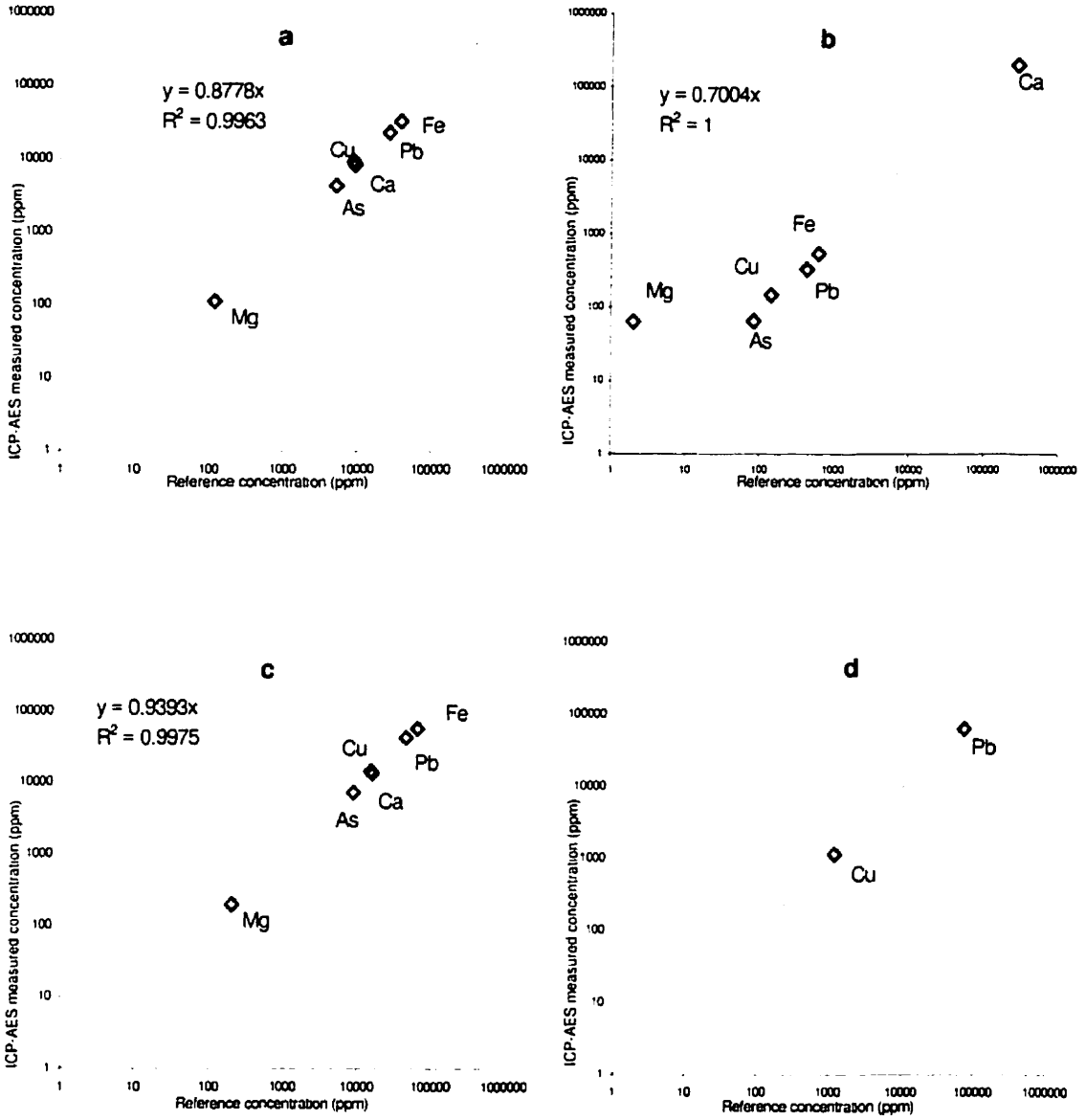

Figure 1.4: Log-log plots comparing mean measured versus expected concentrations for in-house standards PAC (a), GUA (b), and CANMET standards MP-1a (c) and KC-1 (d). Y and R^2 values show the data fit, and results are plotted along a theoretical line with the ideal slope = 1. Decreased y in PAC and GUA compared to MP-1a and KC-1 suggests that smaller sample sizes (0.5 g versus 0.2 g) may improve recoveries. The slight displacement of GUA elements below the 1:1 is due to loss of its MP-1a fraction during preparation of the in-house standard. High measured Mg in GUA is caused by contamination from $CaCO_3$, and was thus treated as an outlier.

Standard	Replicate	Total weight (g)	'g' weight	'g' / Total	$BaSO_4$ Fraction (%)
GUA	1	0.4871	0.0387	7.94	9.00
	2	0.5142	0.0431	8.38	9.00
	3	0.5815	0.0448	7.70	9.00
	4	0.5055	0.0408	8.07	9.00
PAC	1	0.5064	0.1789	35.33	30.00
	4	0.4821	0.1970	40.86	30.00
	5	0.5025	0.1862	37.05	30.00

Table 1.9: Proportion of post-acid digestion residues ('g') with respect to initial total weight, in GUA and PAC. "$BaSO_4$ Fraction" refers to the expected wt. % of $BaSO_4$, based on the preparation of GUA from reagent $BaSO_4$ (see Table 3b). In PAC replicates, the 'g' portion exceeds the expected 30 wt. % of $BaSO_4$ by 5-10%. Precipitated $PbSO_4$ and insoluble SnO_2 (?)accounts for this "extra" weight. In GUA replicates, the 'g' portion falls short of the minimum 9% $BaSO_4$ fraction. This indicates that loss of $BaSO_4$, and possibly $PbSO_4$, has occurred.

Pb Recovery in Standards: Some considerations with respect to digestion

The varying recoveries in the four standards shed light on the behaviour of lead in the chemical environment of acid and Na_2CO_3 digestions. Investigation into this spread in lead recoveries must include a close examination into the digestion process.

HNO_3-HF-$HClO_4$ digestion

Lead was considerably mobile during the digestion process. The percentage of total Pb precipitating as $PbSO_4$ due to HNO_3 oxidation of Pb sulfide, expressed as $\frac{\text{expected Pb in 'g'}}{\text{expected total Pb}}$, is difficult to predict, and varies between replicate samples (Appendix 6). Increased precipitation of $PbSO_4$ correlated with decreased total recovery, (Figure 1.5, *top*) probably because a greater proportion of total Pb was then subjected to further processing in the form of the HF-$HClO_4$ digestion followed by Na_2CO_3 digestion, increasing the risk of loss due to volatilisation, or incomplete digestion by Na_2CO_3.

Rate of $PbSO_4$ precipitation was related to variations in HNO_3 concentration during the first steps of the acid digestion procedure. Taylor (1956) contrasted the products from the reaction of moderate strength HNO_3 + PbS (1) with products from concentrated HNO_3 + PbS (2):

(1) $PbS_{(s)} + 4HNO_{3(aq)} = Pb(NO_3)_{2(aq)} + 2NO_{2(g)} + 2H_2O_{(l)} + S_{(s)}$

(2) $PbS_{(s)} + 8HNO_{3(aq)} = PbSO_{4(s)} + + 8NO_{2\,(g)} + 4H_2O_{(l)}$

Thus samples prewetted with larger volumes H_2O before HNO_3 addition may have precipitated less $PbSO_4$.

However it should be noted that some elemental sulfur in equation (1) may be further oxidised by HNO_3 to produce sulfuric acid, which will in turn react with $Pb(NO_3)_{2(aq)}$ to precipitate $PbSO_4$:

(3) $S_{(s)} + 6HNO_{3(aq)} = H_2SO_{4(aq)} + 6NO_{2(g)} + 2H_2O_{(l)}$

Consequently, $PbSO_4$ is produced to some extent at any given HNO_3 concentration. In addition, the precipitation of $S_{(s)}$ presents other difficulties, to be discussed below.

Sample size may have also had an effect on the proportion of $PbSO_4$ precipitated. Lamothe et al. (1986) improved their Pb recoveries in CANMET ores MP-1a and KC-1 by decreasing sample size from 0.5g to 0.1g. High recoveries from CANMET standards analysed in this study support these findings. KC-1 and MP-1a replicates weighed 0.2g, in contrast to the 0.5g for synthetic rock standards GUA and PAC. Additionally, KC-1 and MP-1a were characterised by a low $\frac{\text{expected Pb in 'g'}}{\text{expected total Pb}}$, indicating a decreased rate of $PbSO_4$ precipitation. Improved recoveries of other elements Ca, Mg, As, Fe (Figure 1.4, this study), Ag, Cu, and Zn (Lamothe et al., 1986) in smaller samples suggests that some overall mechanism other than sulfate precipitation influences element recovery, with respect to sample weight, in sulfide ores.

Losses of Pb during the HNO_3-HF-$HClO_4$ digestion procedure via worker error (e.g. spillage, inaccurate weighing) was unlikely. Cu recovery is a useful indicator of acid digestion technique, because total Cu was conserved in the acid digestion process - i.e., total Cu is present in the "b" solution. Consistently high Cu recoveries (99-106%) from all four standards verify that there were no significant sample losses during the acid digestion procedure.

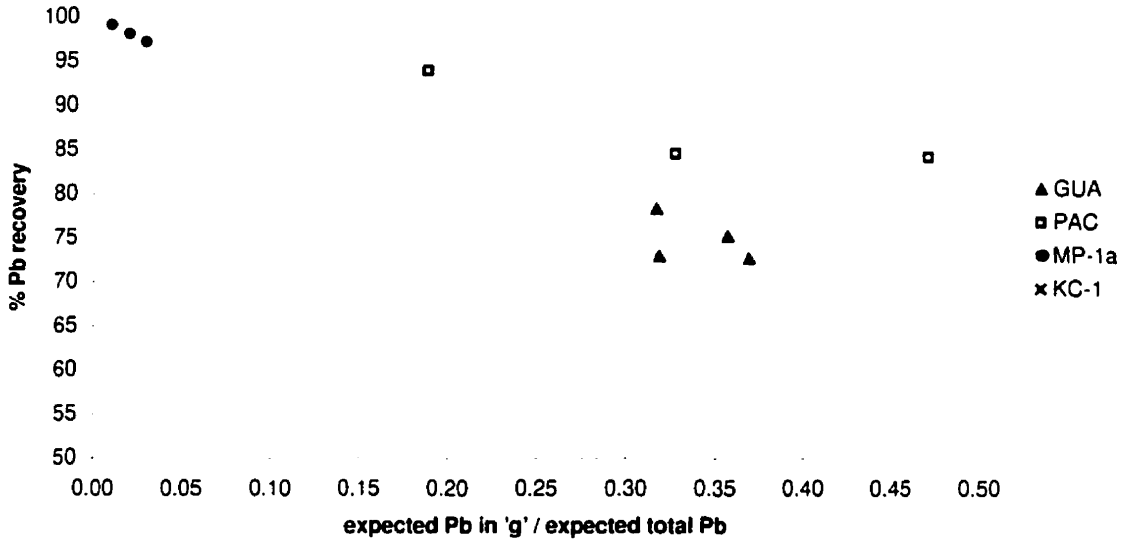

Figure 1.5: Lead recovery versus the proportion of corrected Pb in 'g' to total expected Pb, indicating that improved recovery results from preserving Pb in the 'b' solution by preventing $PbSO_4$ preciptitation. "Expected Pb in 'g'" refers to the difference between the total expected Pb content content and the measured Pb content in the acid-digested 'b' solution. This corrects for any Pb loss during the Na_2CO_3 digestion.

Na_2CO_3 digestion

The spread in Pb recovery between replicates is also due to variations in Na_2CO_3 temperature during the digestion of $(Ba,Pb)SO_4$. The microwave heating routine was kept constant from batch to batch, but variation s in the total liquid load (sum of volume from 12 vessels, Table 1.6) from batch to batch result in heating rates dissimilar from batch to batch and vessel to vessel. Gong et al. (1992b) found that at higher temperatures or due to prolonged heating, the reaction product hydrocerussite ($Pb_3(CO_3)_2(OH)_2$) converted to the less porous $NaPb_2(CO_3)_2(OH)$. A barrier of thickening $NaPb_2(CO_3)_2(OH)$ product layer prevented the inward diffusion of aqueous Na_2CO_3 (Gong et al., 1992a) towards an unreacted $PbSO_4$ core. Thus, the presence of Na in 'g' acts as an indicator of dissolved $NaPb_2(CO_3)_2(OH)$, evidence that the microwave power output promoted heating conditions too extreme for the formation of more porous hydrocerussite (Figure 1.6a).

There is a positive correlation between Pb lost during the Na_2CO_3 digestion, expressed as $\frac{\text{measured Pb in 'g'}}{\text{expected Pb in 'g'}}$, and Na content (Figure 1.6b). The proportion $\frac{\text{measured Pb in 'g'}}{\text{expected Pb in 'g'}}$ (Appendix 6) expresses the efficiency of the Na_2CO_3 digestion , and Figure 1.6b reveals clustering by standard. PAC digestion efficiency is in the range 0.5-0.7; GUA is in the range 0.1-0.35; and the CANMET sulfide ore standards MP-1a and KC-1 fall below 0.1. This behaviour is explained by the barite content of each standard. PAC is 30% (wt.) $BaSO_4$, and the combined barite and $PbSO_4$ content demands the largest volume (~ 40 ml) of Na_2CO_3 for complete digestion. GUA contains 6-9% (wt.) barite, requiring much less (~ 10 ml) Na_2CO_3 solution. Minimal Na_2CO_3 volume (< 5 ml) is required by MP-1a and KC-1 to digest the small amount of $PbSO_4$ precipitate. Smaller

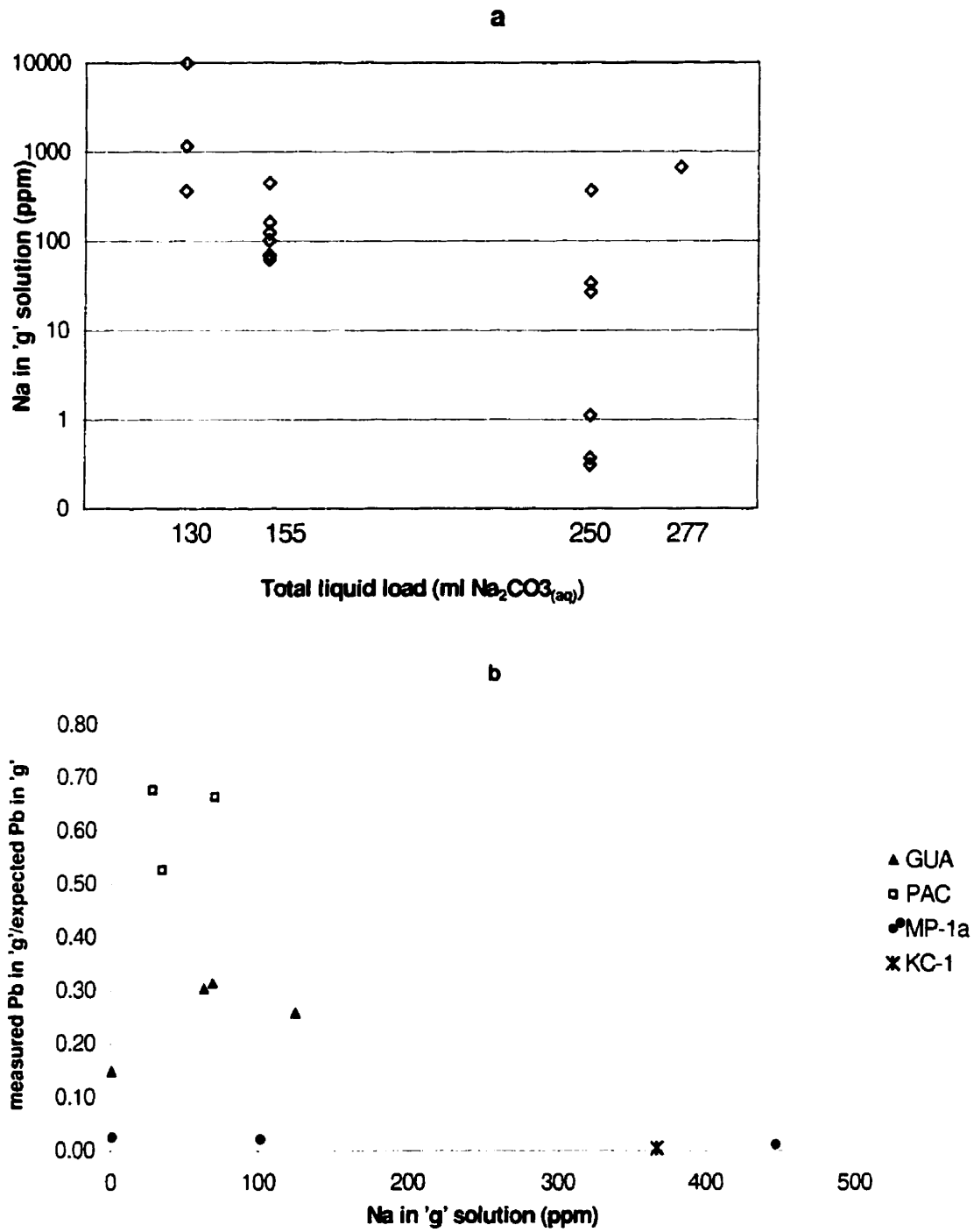

Figure 1.6: (a) Na measured in 'g' solution versus total liquid load during Na_2CO_3 digestion. Elevated Na is found in samples digested in batches with a smaller total liquid volume. **(b)** Measured Pb in 'g'/expected Pb in 'g' versus Na content measured in 'g' This indicates that Pb loss in the 'g' solution is proportional to the 'g' solution's Na content

volumes absorb more heat during the microwave heating cycle, promoting the formation of the $NaPb_2(CO_3)_2(OH)$ product layer. Conversely, the conversion of PAC $PbSO_4$ to lead carbonate proceeds in a cooler environment, resulting in a more successful digestion.

Pb recovery in natural chimneys: some considerations with respect to digestion

Results for bulk analyses of natural chimney and volcanic samples are listed in Tables 2.5, 2.6, and 2.7 in Chapter 2. Large standard deviations among replicates indicate that lead recoveries were highly sensitive to small variations in acid digestion conditions. Two opposing trends with respect to digestion order were observed. Guaymas Basin samples digested in the first batch yielded higher concentrations of all elements, in comparison to the second batch. Conversely, nearly all PACMANUS element concentrations were higher from the first batch.

Replicates of PACMANUS subsample 118693-1 (henceforth referred to as P1) were included in every digestion batch as an internal standard. Replicate P1-2 was prewetted with increased volumes of water. After the HNO_3 digestion, the insoluble residues observed in P1-1 (i.e., P1, batch 1) were dissimilar to those seen in P1-2 (P1, batch 2 replicate). Visible elemental sulfur was present in P1-2 (Figure 1.7).

In theory (Taylor, 1956), the formation of sulfur as a product of the reaction between HNO_3 and metal sulfides is favourable, since it is associated with decreased precipitation of $PbSO_4$. However, other mechanisms, both chemical and mechanical, may ultimately decrease recoveries in sulfur-forming digestion reactions. In a sulfide-rich environment, some sulfur may be further oxidized by excess HNO_3, producing H_2SO_4. This sulfuric acid is free to react with $Pb(NO_3)_{2(aq)}$ to precipitate $PbSO_4$.

(3) $S_{(s)} + 6\ HNO_{3\ (aq)} \Rightarrow H_2SO_{4(aq)} + 6NO_{2(g)} + 2H_2O_{(l)}$

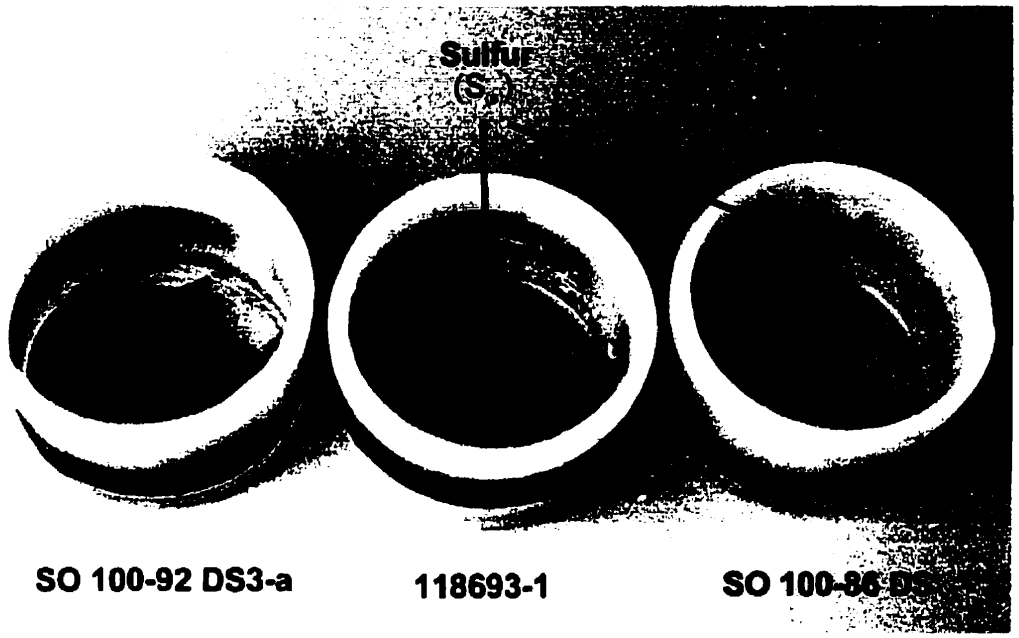

Figure 1.7 : 60 ml Teflon digestion vessels containing residues after digestion with moderate strength HNO_3 : (*Left*), PAR volcanic SO 100-92 DS-a; (*Centre*), PACMANUS subsample 118693-1, exhibiting a green solution due to high Cu content, and a yellow elemental sulfur ($S_{(s)}$)precipitate adhering to the vessel wall; (*Right*) elemental sulfur had also formed on vessel walls in the sulfide-rich PAR sample SO 100-86 DS (not included in this study).

(4) $H_2SO_{4(aq)} + Pb(NO_3)_{2(aq)} \Rightarrow PbSO_{4(s)} + 2H_2O_{(l)} + 2NO_2$

Secondly, sulfur was observed to clump together and adhere to vessel walls. These clumps conceivably may have trapped lead sulfate particles, 'immunizing' them from further digestion. The sulfide-rich PACMANUS chimneys require concentrated HNO_3 to avoid $S_{(s)}$ precipitation.

Chimney material from Guaymas Basin showed *lower* recoveries in the first batch of digestions. This effect was most pronounced in the carbonate-sulfate chimneys containing minor sulfides. Lower recoveries were associated with a higher mass of sulfate precipitates, suggesting that moderate (11 M) HNO_3 concentrations are better suited to carbonate-bearing, low-sulfide chimneys.

CONCLUSIONS

Four standards were digested by HNO_3-HF-$HClO_4$, followed by digestion with a microwave-heated aqueous Na_2CO_3 solution. Recoveries averaged 88% from in-house standard PAC and 91%-98% from CANMET ore standards. Poor recovery (25% loss) from in-house standard GUA was attributed to error in standard preparation.

Tests of the effect of high Ca on Pb emission signals were inconclusive. The typical suppression effect (Boss and Freeden, 1989) was not observed. Instead, measurement of calcium-spiked standards showed a 20% enhancement of Pb emission signal. This effect was also observed in other elements in standard s3, including Fe, Mn, Ni, and Co (Table 1.3), suggesting that it cannot be attributed to an oxide-formation or ionization effect. The effect of Ca concentrations higher than 990 μg/ml is unknown, however. GUA standard solutions containing approximately 5600 μg/ml Ca may have experienced Pb suppression not apparent at lower Ca concentrations.

Lead recovery was influenced by variations in HNO_3 concentration, as well as variations in the temperature of the heated Na_2CO_3 solutions during digestion. Precipitation of $PbSO_4$ correlated with decreased total recovery. The formation of less-porous $NaPb_2(CO_3)_2(OH)$ over hydrocerussite ($Pb_3(CO_3)_2(OH)_2$) during the Na_2CO_3 digestion was associated with lead loss.

This method can be modified to expand its capability for multi-element determinations. The inclusion of aqua regia (HCl-HNO_3 in the proportion 3:1) in the digestion procedure would ensure that the gold in solution represents total gold (M.P. Gorton, University of Toronto, personal communication, 1997). Also inherent in its present form, is the inability of the method to provide quantitative analyses of barite by ICP. It is understood that the "sulfate" solution is

composed not only of hydrothermal barite, but also the chemical precipitate $PbSO_4$, a product of the HNO_3 digestion procedure. A pre-digestion step with HCl, a non-oxidizing acid, may decompose sulfides without the resulting precipitation of $PbSO_4$ (M.P. Gorton, University of Toronto, personal communication, 1997). Any chloride precipitates, including PbCl, may be treated with the subsequent $HF\text{-}HClO_4$ step. This digestion may produce a "clean" barite, which can be then analyzed quantitatively.

To further shorten preparation times, microwave-assisted $HNO_3\text{-}HF\text{-}HClO_4$ digestion (Nakashima et al., 1988; Chao and Sanzolone 1992; Fadda and Rivoldini, 1995) of seafloor material is possible with a microwave oven equipped to handle venting of acid fumes.

The ease of volatilisation that characterises Pb is central to the problem of obtaining accurate lead analyses. Lamothe et al. (1986) attributed their good recoveries to the use of a sealed digestion vessel, thus preventing Pb volatilisation. Additionally, it is recommended that future Na_2CO_3 digestions be performed within sealed, non-vented Teflon bombs, to prevent losses through leakage or venting.

The microwave-heated Na_2CO_3 digestion procedure provides a rapid method for the decomposition of refractory sulfates, cutting sulfate decomposition time from hours or days down to less than 1 hour. It is a viable alternative to decomposition by furnace-heated aqueous Na_2CO_3 or traditional fusion methods, both of which are considerably more time-consuming. Natural barite and anglesite, as well as sulfates precipitated during acid digestion, can be digested and included in ICP-AES/ICP-MS/AAS bulk analyses for major and trace elements. This method is especially suited to the study of hydrothermal vent material, due to their characteristically barite-rich and sulfide-rich nature. The use of a temperature-feedback microwave system is recommended for future work. The correlation of power output to time-

temperature will quantify the parameters of the microwave sulfate digestion technique, improving the reproducibility of the method (Kingston and Haswell, 1997). Close temperature control would ensure that reaction conditions favour the formation of the more porous hydrocerussite ($Pb_3(CO_3)_2(OH)_2$) over $NaPb_2(CO_3)_2(OH)$.

Overall, the improvement of sample digestion techniques is highly relevant to the study of black smoker geochemistry. Analysis by ICP-AES/ICP-MS/AAS permits sample weights (0.1-0.5g) much smaller than those required by XRF (3-5 g). In light of the time-consuming, high-cost seafaring expeditions necessary to recover small volumes of material from the seafloor, this is practical advantage.

REFERENCES

Binns, R.A., Scott, S.D., Bogdanov, Y.A., Lisitzin, A.P., Gordeev, V.V., Gurvich, E.G., Finlayson, E.J., Boyd, T., Dotter, L.E., Wheller, G.E., Muravyev, K.G. (1993): Hydrothermal oxide and gold-rich sulfate deposits of Franklin Seamount, Western Woodlark Basin, Papua New Guinea. Economic Geology 88(8), 2099-2121.

Boss, Charles B. and Freeden, Kenneth, J. (1989): Concepts, Instrumentation, and Techniques in Inductively Coupled Plasma Atomic Emission Spectrometry. The Perkin-Elmer Corporation

Breit, G.N., Simmons, E.C. & Goldhaber, M.B. (1985): Dissolution of barite for the analysis of strontium isotopes and other chemical and isotopic variations using aqueous sodium carbonate. Chemical Geology (Isotope Geoscience Section) 52, 333-336.

Castillejos, E.A.H., de la Cruz del B., F.P., Uribe S., A. (1996): The direct conversion of celestite to strontium carbonate in sodium carbonate aqueous media. Hydrometallurgy 40(1-2), 207-222.

Chao, T.T. and Sanzolone, R.F. (1992): Decomposition Techniques. In: Geoanalysis (Special Issue). Journal of Geochemical Exploration, Vol 44.

Chen, T.T., and Dutrizac, J.E. (1996): The mineralogical characterization of lead-acid battery paste. Hydrometallury, 40 (1-2), 223-245

Fadda, S., Rivoldini, A. ICP-MS def.... Geostandards Newsletter. Vol. XIX, No.1. April 1995.

Faye, G.H., Bowman, W.S. and Sutarno, R. (1974): Zinc-lead-tin-silver ore KC-1: Its Preparation and Characterization for use as a Certified Reference Material. Technical Bulletin TB 193. Energy, Mines and Resources Canada.

Gong, Y., Dutrizac, J.E., Chen, T.T. (1992a): The conversion of lead sulfate to lead carbonate in sodium carbonate media. Hydrometallurgy 28(3), 399-421.

_____(1992b): The reaction of anglesite ($PbSO_4$) crystals with sodium carbonate solutions. Hydrometallurgy 31(3), 175-199.

Hannington, M.D. (1986): Geology, mineralogy, and geochemistry of a sillica-sulfate-sulfide deposit, Axial Seamount, N.E. Pacific Ocean. M.Sc. thesis, University of Toronto

Harris, Daniel C. Quantitative Chemical Analysis (1991). W.H. Freeman and Company, New York. 3rd ed.

Herzig, P.M., Hannington, M.D. and Arribas Jr., A (1996): Submarine gold mineralization in the New Island Fore-Arc, Papua New Guinea. Supplement to *EOS, Transactions*, American Geophysical Union, May 28, 1996; Vol. 77(22), p.W120

King, Edward E. and Barclay, David. A microwave chemistry system for the laboratory. American Laboratory. October 1997. 27-30.

Kingston, H.M. and S.J. Haswell (1997): Microwave-Enhanced Chemistry: Fundamentals, Sample Preparation, and Applications. American Chemical Society; Washington, D.C.

Lamothe, P.J., Fries, T.L. and Consul, J.J. (1986): Evaluation of a microwave oven system for the dissolution of geologic samples. Analytical Chemistry (58) 1881-1886.

Mahan, Kent I., Foderaro, Tom A., Garza, Tressa L., Martinez, Russel M., Maroney, Gary A., Trivisonno, Mike R. and Willging, Ellen M. Microwave Digestion of Techniques in the Sequential extraction of calcium, iron, chromium, manganese, lead, and zinc in sediments. Analytical Chemistry, 1987, 59, 938-945.

Nakashima, Susumu, Sturgeon Ralph E., Willie, Scott N., Berman, Shier, S. (1988): Acid digestion of marine samples for trace element analysis using microwave heating. Analyst, January 1988 vol.113, 159-163.

Nakdarni, R.A. (1984): Applications of microwave oven sample dissolution in analysis. Analytical Chemistry, 1984. Vol. 56: 2233-2236.

Ontario Geological Survey (1990): The Analysis of Geological Materials, Volume II: A Manual of Methods. Ontario Geological Survey Miscellaneous Paper 149. Ministry of Northern Development and Mines, Ontario.

Parisot, S. (1997): Echanges asthènosphere-lithosphere-océan: Gèochimie des processus hydrothermaux. Université Bretagne Occidentale. Rapport de DEA 96-97, Geochimie-Metallogenie, 39 p., unpublished.

Puchelt, H. & Setiobudi I.J. (1989): New dissolution technique for rarely soluble sulfate minerals for AAS and ICP investigations. Fresenius Z. Anal. Chem. (335), 69^{2}-694.

Rona, P. Hydrothermal mineralization at oceanic ridges. Canadian Mineralogist. Vol. 26, part 3. 1987

Scott, S.D. (1997): Submarine hydrothermal deposits and systems. *In*: Geochemistry of Hydrothermal Ore Deposits, H.L. Barnes, ed., John Wiley & Sons, 3rd edition, p. 797-875.

Sen Gupta, J.G. (1987): Determination of rubidium, strontium and barium in barite by atomic-absorption spectrometry after dissolution in disodium ethylenediaminetetra-acetate. Talanta. 34(4), 427-431.

Sen Gupta, J.G. (1991): Determination of barium, strontium and nine minor and trace elements in impure barite and strontianite by inductively-coupled plasma atomic emission spectrometry after dissolution in disodium ethylenediaminetetraacetate. Talanta. 38(10), 1083-1087.

Smith, F. and Cousins, B. (1985) The acid dissolution of sulfide mineral samples under pressure in a microwave oven. Analytica Chimica Acta, 177: 243-245.

Steger, H.F. and Bowman, W.S. (1982): MP-1a: A Certified Reference Ore. CANMET Report 82-14E. Canada Centre for Mineral and Energy Technology.

Taylor, F.S. (1956) Inorganic and Theoretical Chemistry. 9th edition. William Heinemann, Ltd.

Totland, Marina, Jarvis, Ian and Jarvis, Kym. (1992) An assessment of dissolution techniques for the analysis of geological samples by plasma spectrometry. Chemical Geology, 95 (1992); 35-62.

Weast, Robert C. and Astle, Melvin J.,eds. (1983) CRC Handbook of Chemistry and Physics. CRC Press, Inc., 63rd ed.

CHAPTER 2:

Pb CONTENT AND DISTRIBUTION IN SEAFLOOR HYDROTHERMAL CHIMNEYS FROM GUAYMAS BASIN, GULF OF CALIFORNIA; PACMANUS, EASTERN MANUS BASIN; AND THE SOUTHERN EAST PACIFIC RISE

INTRODUCTION

The distribution and concentration of lead in hydrothermal deposits and its global recycling is not well understood. This is due in large part to the paucity of reliable lead analyses. This study examines the geochemistry of lead in hydrothermal chimneys from three contrasting tectonic environments. At the PACMANUS site, a Cu-Zn-Pb-Ag-Au deposit is hosted by felsic volcanics in a back-arc basin. At Guaymas Basin, Fe-Cu-Zn-Pb deposits are forming on a heavily sedimented spreading ridge axis. A small suite of volcanics and massive sulfides from the super-fast-spreading southern East Pacific Rise region was also included in the study.

Several studies have been conducted on the nature of lead in marine metalliferous sediments. Peucker et al. (1994) noted a surplus of lead in the continental crust while performing mantle-continental crust mass-balance calculations. They concluded that hydrothermal transfer of lead from the mantle to metalliferous sediment accounted for this surplus. However, they noted that their calculations did not take into account the possible contribution from massive sulfides and stockwork ores at active seafloor vents. If high lead concentrations are present in large volumes of seafloor sulfides, these may also account for some of the surplus of lead found in the continental crust.

Although this study focuses very specifically on the small-scale distribution of lead within a chimney, it should lead to a larger-scale understanding of the behaviour of lead in the

GEOLOGICAL SETTINGS

The hydrothermal deposits at Guaymas Basin are located within an active seafloor-spreading segment (Lonsdale et al., 1980) in the Gulf of California (Figure 2.1, *top* and *bottom*). Hydrothermal fluids circulate through a blanket of sediment up to 500 m thick. The sediments are both terrigenous, originating from Mexican volcanics (Peter and Scott, 1988), and biogenic in composition. The latter results in a high organic carbon content of 3-4% in the sediment (Peter and Scott, 1988). Alteration in basaltic sills that intercalate with, and underlie, the sediments suggests hydrothermal fluid-basalt interaction (Peter and Shanks, 1992) as well. The hydrothermal venting site is located at a water depth of 2000 m. Guaymas Basin chimneys are unusual for their calcite abundance and the hydrocarbons that impregnate mound and chimney material (Peter and Scott, 1988; Peter et al., 1991).

The PACMANUS deposit sits on the volcanically active, Y-shaped Pual Ridge in the eastern Manus Basin, a pull-apart structure within the Manus back-arc system of Papua New Guinea (Figure 2.2). Lava domes ranging from dacitic to rhyodacitic in composition (Binns and Scott 1993) host the hydrothermal vent sites. The hydrothermal field is distributed over an area of 800 × 350 m and at a water depth of 1650-1675 m (Scott and Binns, 1995). The mineralogy of massive sulfide-sulfate chimneys is typical for deposits forming in a back-arc setting, and they are generally enriched in Cu, Zn, Pb, Ag and Au. Several hydrothermal sites have been identified within the PACMANUS area, including Satanic Mills, an active high temperature site. Roger's Ruins is an older, inactive site approximately 900 m to the north of Satanic Mills.

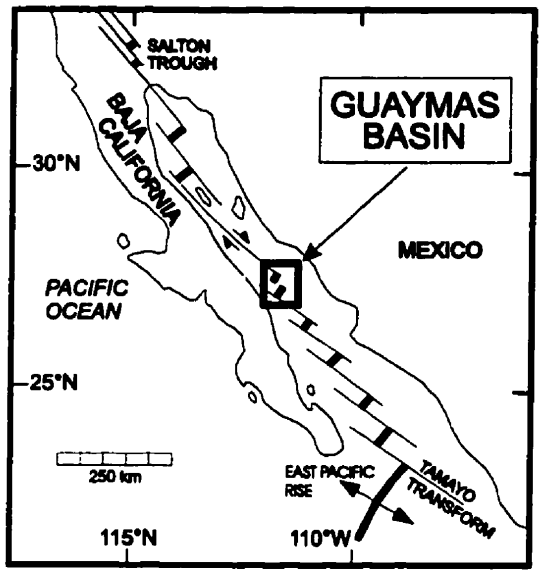

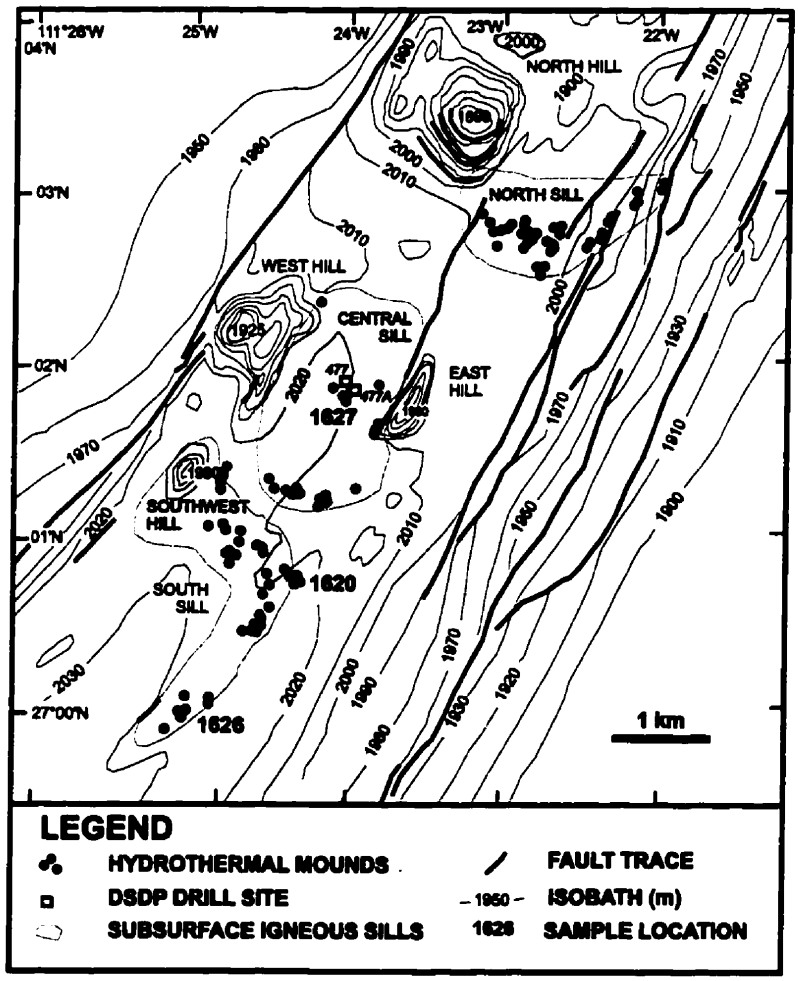

Figure 2.1: Location map for Guaymas Basin, Gulf of California (*top*); Map showing location and distribution of main hydrothermal mounds (*bottom*), with locations for dives 1620, 1626 and 1627 shown. (Modified from Peter et al., 1991)

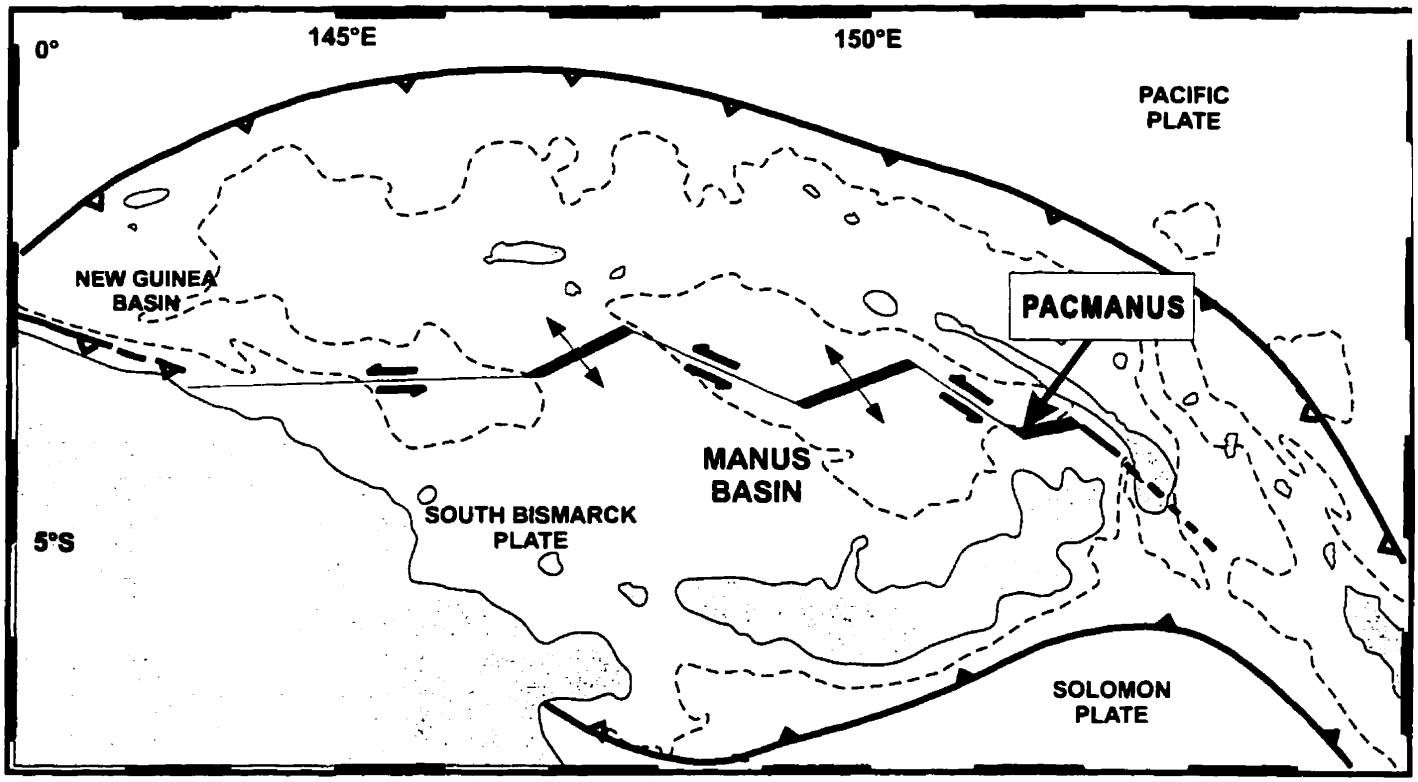

Figure 2.2: Location of the PACMANUS hydrothermal vent field within the Manus Basin. (Modified from Moss et al., 1997 and Moss, unpubl.)

The southern segment of the East Pacific Rise is a super-fast spreading ridge (11-15 cm/yr), forming at the junction of the Pacific Plate, Nazca Plate and the Juan Fernandez Microplate (Figure 2.3, *left*). Pito Deep, located along the Easter microplate, is a large depression (5985 m depth) at the tip of a ridge propagator of the East Rift (Constantin et al. 1996). Basalts and diabase dykes overlie the lower-crust lithologies, consisting mainly of massive olivine-bearing gabbros.

The PAR (Pacific-Antarctic Ridge) axial region, consists of several en echelon ridge segments, south of the Juan Fernandez microplate (Figure 2.3, *right*). The system is notable for its felsic volcanics, which are host to active hydrothermal venting. These dacites (60-65% SiO_2) and andesites (55-59% SiO_2) form glassy sheet flows and highly vesicular pillow lavas. Dacite mineralogy is typically plagioclase (An_{35-50}), Mg-poor olivine and titanomagnetite. MORB and Fe-Ti basalts are also present. The ridge crest is nearly 1 km wide and depths range from 2230 m to 2650 m (Hékinian et al. 1997).

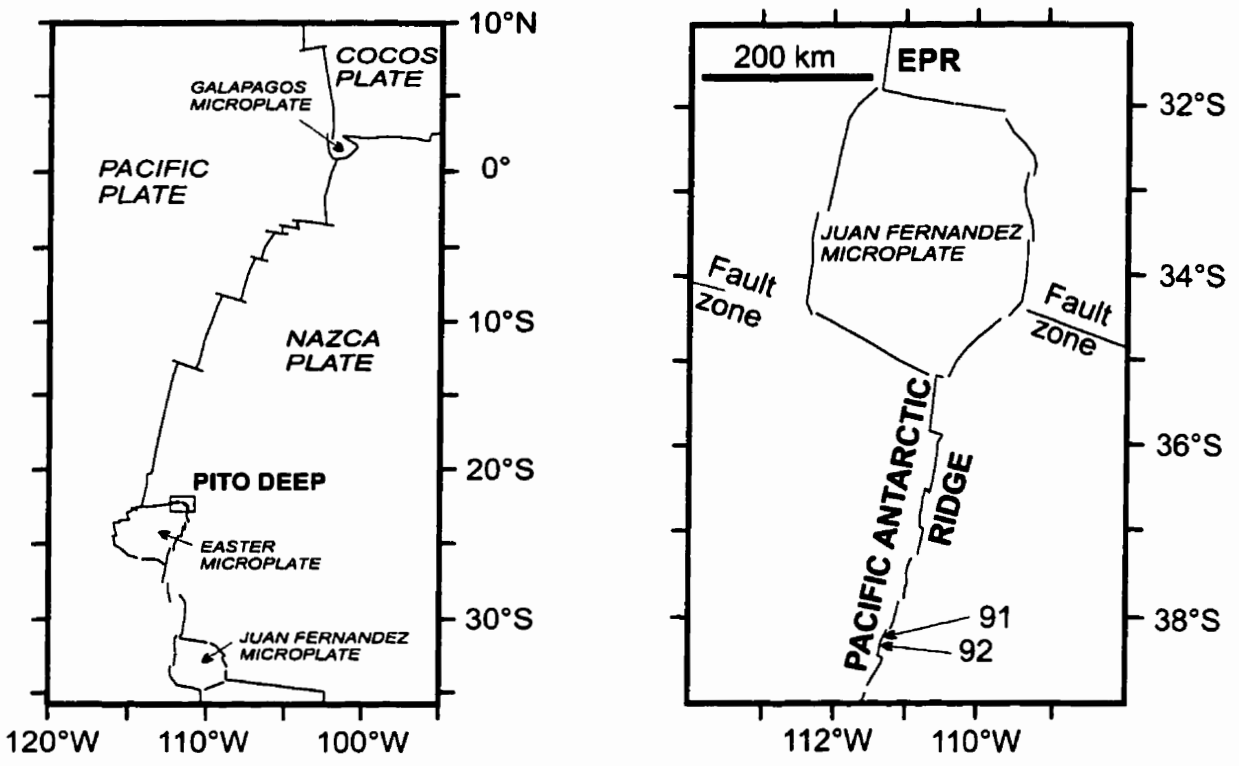

Figure 2.3: Location map for Pito Deep, located along the Easter Microplate (left) (Modified from Constantin et al., 1996). Close-up of the Juan Fernandez Microplate and the Pacific Antarctic Ridge (PAR), showing the locations of Sonne dredges 91 and 92 (right). (Modified from Hekinian et al., 1997)

METHOD

Analytical Methods

A suite of active and inactive chimneys and mound material was obtained from these four separate hydrothermal sites (Table 2.1). Based on mineral assemblage, all chimneys were classified as sulfate-carbonate, sulfide-sulfate, or massive-sulfide (Table 2.2). Subsamples across the chimneys were taken for bulk analysis by INAA and ICP-AES. Polished thin sections cross-sectioning chimney walls were examined. Elemental X-ray maps and BSE images were collected by electron microprobe.

TABLE 2.1: Chimneys and volcanic rock from Eastern Manus Basin, Guaymas Basin, and southern East Pacific Rise

Dive/Dredge	Sample	Cruise, Site	Description
Pual Ridge, Eastern Manus Basin			
MD-35	118693	PACMANUS II	Cross-section slab through mid-upper section of very large inactive (?) chimney 118579, Nicknamed "Fred"; Zn-Cu sulfide-rich
MD-62	132452	PACMANUS III, Satanic Mills	Sphalerite-anhydrite rich sulfide fragments; minor chalcopyrite + hematite
MD-59	132744	PACMANUS III, Roger's Ruins	Large fragment of partially oxidised massive sulfide chimney
Southern trough, Guaymas Basin			
1620	C1	ALVIN 1985	Active mound, excavated to allow sampling of 307°-309°C hydrothermal fluids
1626	A1	ALVIN 1985	Chimney venting 176°C fluid
1627	A3	ALVIN 1985	Fragment from base of an active, high temperature chimney. Inner wall is chalcopyrite-sphalerite rich, with anhydrite on outer wall
1966	A	ALVIN 1988	Chimney fragment collected at depth 2012 m, at 27°00'N, 111°24'W
Pito Deep, Easter Microplate			
PI-07	07	Pito Deep	Sulfide (pyrite, marcasite) + sulfate (anhydrite?) + Fe-oxides
PI-07	10a	Pito Deep	Small chimney piece (1.5 cm wide); interior wall well-crystallized; pyrite/marcasite; followed by ZnS zone; followed by pyrite + ZnS zone; Fe-oxide on outer wall
Pacific-Antarctic Ridge			
SO 100-91	DS	R/V *Sonne* Leg 100	Dacite; black fresh glass; rare vesicles
SO 100-91	DS1	R/V *Sonne* Leg 100	Dacite; same as SO 100-91 DS
SO 100-92	DS3-a	R/V *Sonne* Leg 100	Black glass with staining
SO 100-92	DS3-b	R/V *Sonne* Leg 100	Aphyric black volcanic; rare vesicles; minor glass, some Fe-staining
SO 100-92	DS3-c	R/V *Sonne* Leg 100	Fresh unaltered black volcanic glass; shiny lustre

TABLE 2.2: Classification of Chimney types

Location	Chimney Type	Chimney	Mineral Assemblage
Guaymas Basin	Carbonate-sulfate	1620-C1	ca-anh-ba-sp-(ga)
		1626-A1	anh-ba-ca-(ga)
		1966-A	ca-ba-sp-po-ga
	Massive sulfide	1627-A3	sp-cpy-bn-anh
PACMANUS	Massive sulfide-sulfate	118693	sp-ba-mc-py-cpy-anh
		132452	sp-anh-(cpy-hm)
	Oxidized sulfide-sulfate	132744	oxidized Fe, Zn sulfides

Legend:

anh	anhydrite
ba	barite
ca	calcite
cpy	chalcopyrite
ga	galena
hm	hematite
mc	marcasite
po	pyrrhotite
py	pyrite
sp	sphalerite/wurzite
( )	trace

Sampling Methods

Table 2.3 lists all subsamples from PACMANUS and Guaymas Basin chimneys.

A cross-section slab was cut midway up a large inactive (?) PACMANUS chimney (Figure 2.4), dredged during the PACMANUS II expedition. Based on the preliminary study of two large polished thin sections (A and B, Figure 2.5), chimney 118693 ("Fred") was divided into eight distinct mineralogical zones, from the high-temperature Zone 1, located at the chimney's centre, out to the oxidized Zone 8 on the outer chimney wall (Figure 2.6a). Six subsamples were taken along a radius for bulk analyses (Figure 2.6b). The subsamples were crushed to 2mm rock chips, then ground using an alumina mill. The alumina mill was scoured with quartz sand between each sample to prevent cross-contamination. Portions of two other PACMANUS chimney fragments (132452 and 132744), dredged during the PACMANUS III expedition, were also crushed and powdered for bulk analysis.

A small suite of carbonate-sulfate and sulfide chimneys from Guaymas Basin was obtained from J. Peter (GSC, Ottawa). Three chimneys of the carbonate-sulfate type (Figures 2.7a, b, c) were collected during the 1985 ALVIN dives to the site. The sulfide-rich inner wall of each chimney was subsampled using a hand drill. Some subsamples were extremely friable and easily powdered with an agate mortar and pestle. A fourth chimney, 1627-A3 (Figure 2.7d), was selected for its sulfide-rich content, atypical for Guaymas Basin material. It was cut using a dry saw, crushed to 2mm chips, and ground using an alumina mill.

In addition, five dacite and two massive sulfide rock powders, collected from Southern East Pacific Rise by Nautile submersible, were obtained from R. Hékinian (IFREMER, France) and analysed by ICP-AES.

TABLE 2.3: PACMANUS and Guaymas Basin subsamples analysed by ICP-AES

Subsample	Location	Description
118693-1	PACMANUS	Central conduit, 118693
118693-2	PACMANUS	Midsection, 118693
118693-3	PACMANUS	Midsection, 118693
118693-4	PACMANUS	Midsection, 118693
118693-5	PACMANUS	Outer wall, 118693
118693-6	PACMANUS	Outer wall, 118693
1620-C1-1	Guaymas Basin	Inner wall, 1620-C1
1620-C1-2	Guaymas Basin	Outer wall, 1620-C1
1626-A1-1	Guaymas Basin	Inner wall, 1626-A1
1626-A1-2	Guaymas Basin	Outer wall, 1926-A1
1627-A3-1	Guaymas Basin	Inner wall, 1627-A3
1627-A3-2	Guaymas Basin	Midsection, 1627-A3
1627-A3-3	Guaymas Basin	Outer wall, 1627-A3
1966-A-1	Guaymas Basin	Inner wall, 1966-A
1966-A-2	Guaymas Basin	Outer wall, 1966-A

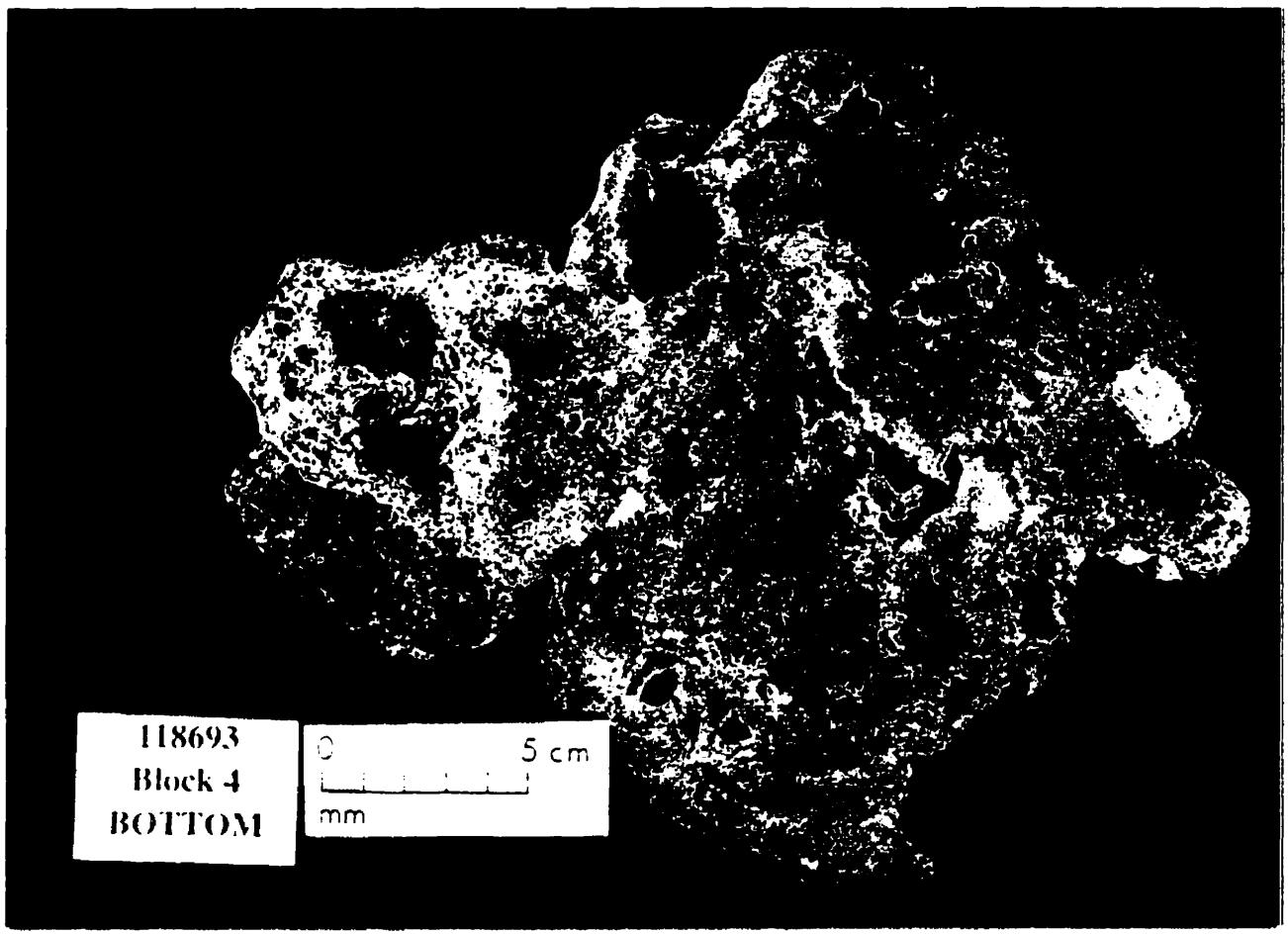

Figure 2.4: Cross-section cut midway through PACMANUS chimney 118693 ("Fred")

Figure 2.5: Cross-section through 118693 ("Fred")
Bottom view
PACMANUS, eastern Manus Basin

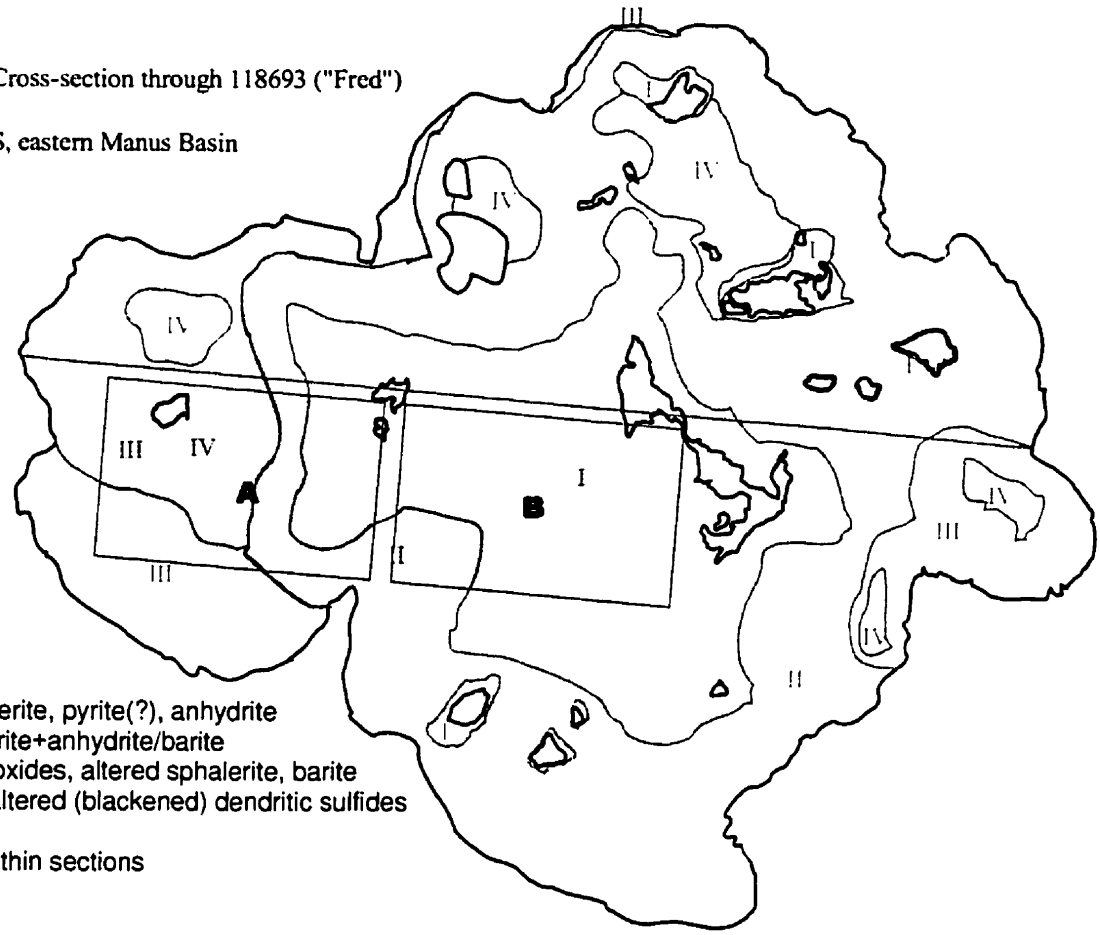

LEGEND

I - cpy +/- sphalerite, pyrite(?), anhydrite
II - sulfides - pyrite+anhydrite/barite
III - porous Fe-oxides, altered sphalerite, barite
IV - vug infills: altered (blackened) dendritic sulfides

A, B - polished thin sections

Figure 2.6a: 8 Mineralogical Zones from 118693 ("Fred"), PACMANUS site. These Zones were identified across thin sections A and B.

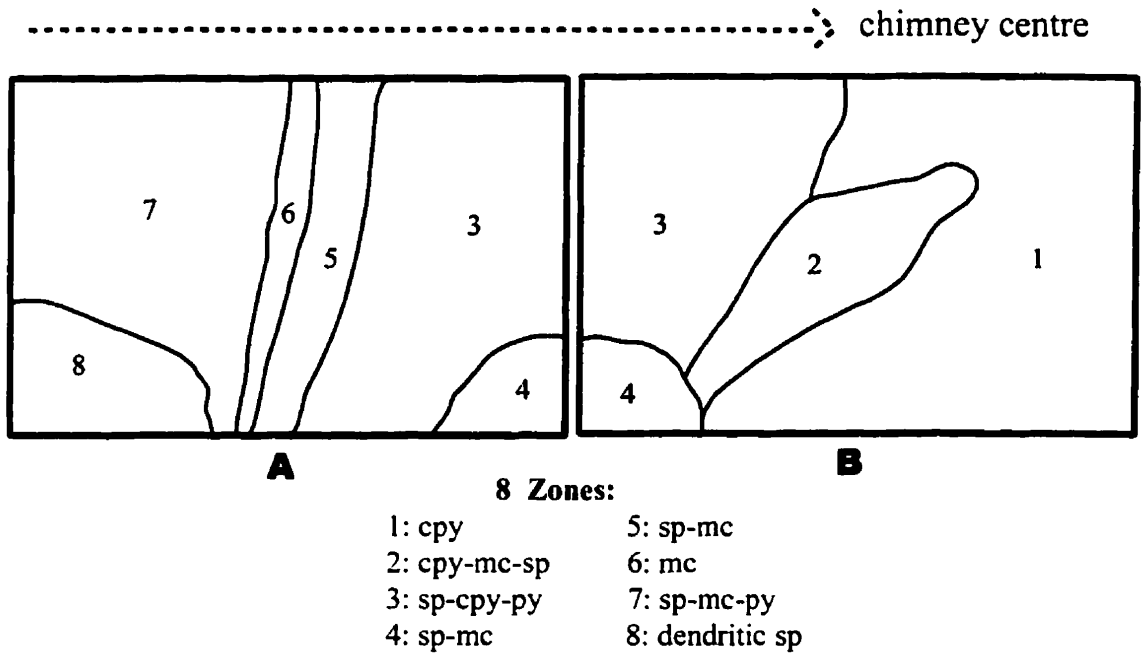

Figure 2.6b: Six subsamples cut from 116693 for bulk analysis by ICP-AES and INAA. Each subsample is representative of one or two of the mineralogical Zones, as shown above.

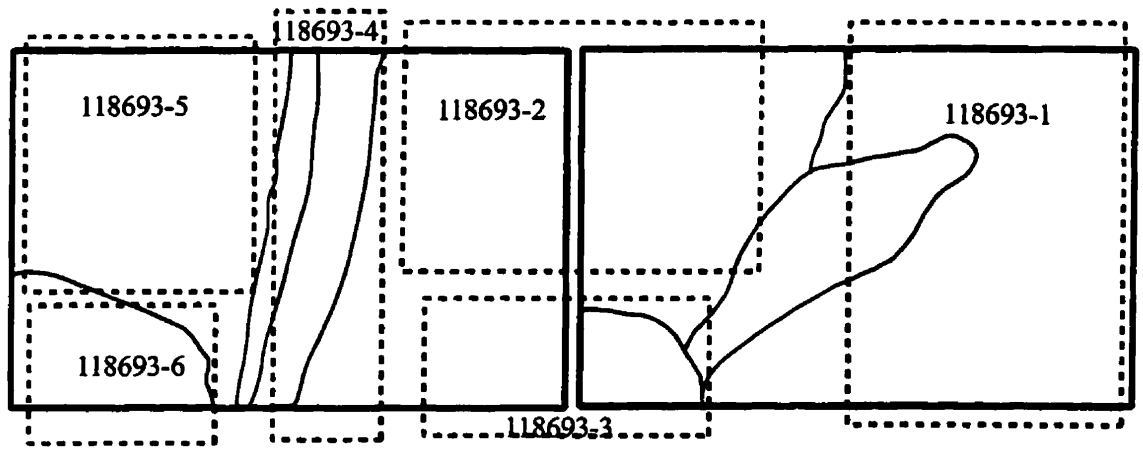

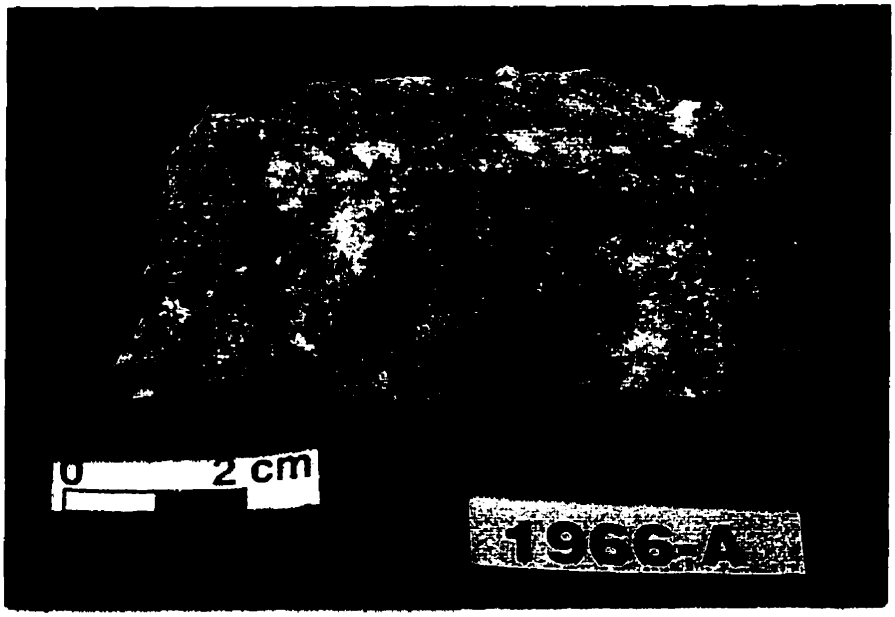

Figure 2.7a: Guaymas Basin chimney 1620-C1. The inner conduit (dark grey) is lined with sphalerite-pyrrhotite-(galena). Barite and calcite (light grey, white) make up the outer wall.

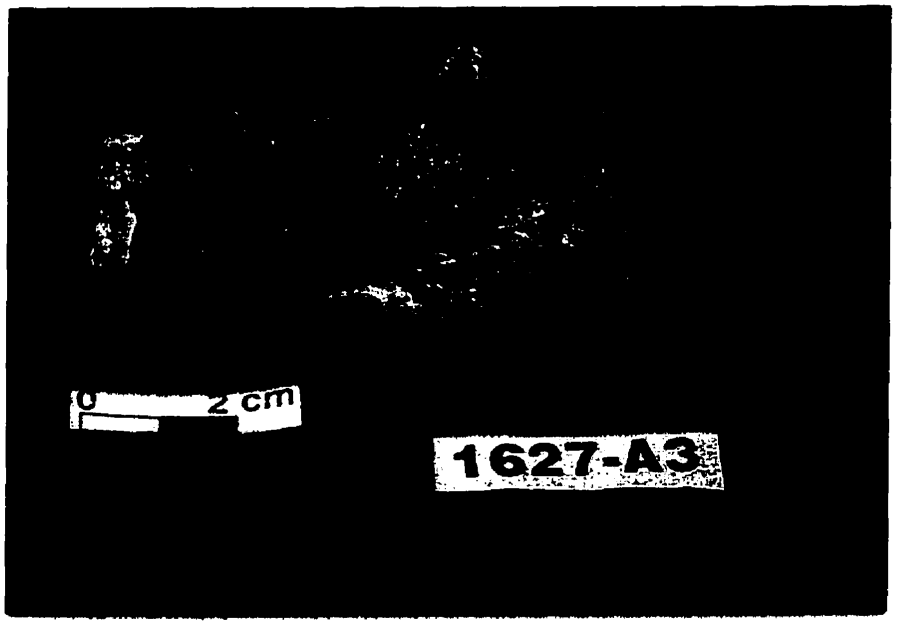

Figure 2.7b: Guaymas Basin chimney 1626-A1. The inner conduit (dark grey) is lined with sphalerite-pyrrhotite-(galena). Barite and carbonate (brown, white) make up the outer wall.

Figure 2.7c: Guaymas Basin chimney fragment 1966-A. An inner conduit (dark grey) is lined with sphalerite-pyrrhotite-(galena). Barite and carbonate (mottled brown, grey, white) make up the outer wall.

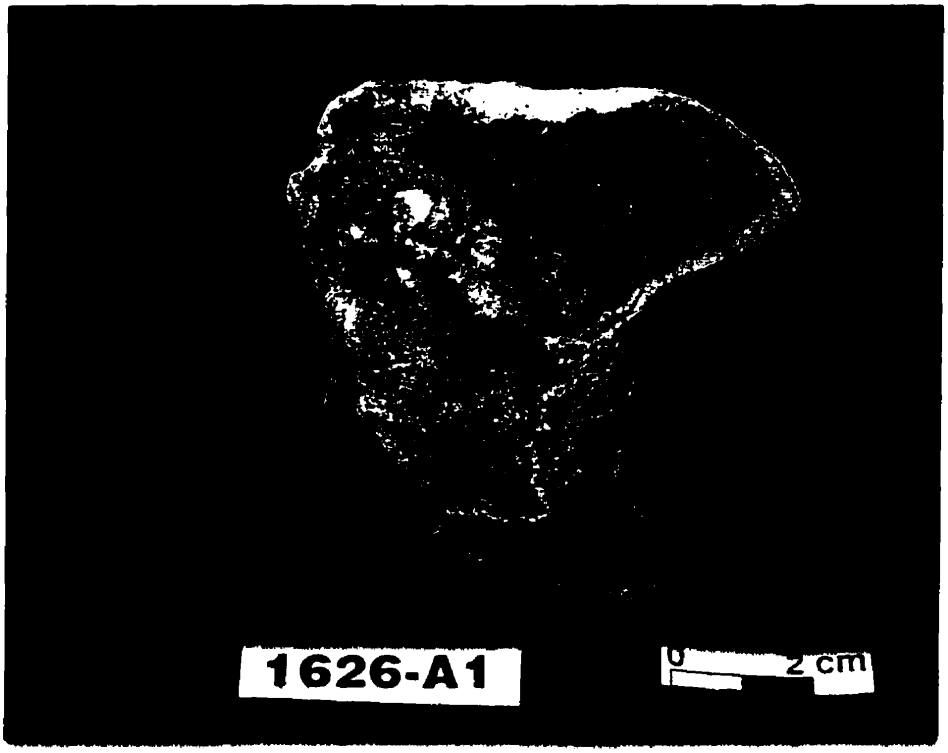

Figure 2.7d: Guaymas Basin chimney 1627-A3. Concentric bands of massive sphalerite (dark grey) alternate with chalcopyrite (yellow), bornite (blue-grey), and other Cu sulfides. Minor anhydrite + calcite (?) is also visible.

MINERALOGY

PACMANUS deposit

The characteristic mineralogy and chimney paragenesis of PACMANUS massive sulfides is detailed in Parr et al. (1996). The following is a summary of textures and associations observed in chimney 118693.

Massive chalcopyrite comprises 90% of Zone 1 and lines conduit walls (Figure 2.5) throughout the chimney. Aggregates of subhedral, angular grains form in Zones 2 to 5, occasionally intergrown with marcasite and sphalerite. Abundance decreases outward to trace relict grains in Zones 5. Chalcopyrite is replaced by colloform sphalerite in Zones 3 and 4.

Internal reflections in sphalerite are characterized by a gradual progression from deep red-orange in Zones 1 and 2, to yellow-orange in Zones 5 and 6, indicating an outwardly decreasing Fe:Zn ratio. Individual grains of sphalerite in Zones 7 and 8 are increasingly iron-rich from core to outer rim. Inner zones are characterized by massive sphalerite, which progresses to colloform and massive sphalerite in middle zones; and dendritic sphalerite in the porous outer zones.

Marcasite, most abundant in zones 2, 4 and 6, occurs as porous, cream-coloured (in reflected light) radial aggregates, partly replaced by chalcopyrite in central zones. Later generations of marcasite are "cleaner" in appearance. Colloform marcasite in the transitional Zone 6 grows outward and is replaced by fresher subhedral marcasite.

Pyrite generally forms subhedral grains, exhibiting caries texture as they are replaced by chalcopyrite or Pb-As sulfosalts. Spheroid pyrite forms with dendritic sphalerite in Zones 7 and 8.

Tetrahedrite commonly forms euhedral triangular grains that are either enclosed in massive sphalerite, or protrude into open cavities (Figure 2.8b). Blebs form along contacts between chalcopyrite and marcasite, and appear to be replaced by chalcopyrite.

Pb-As sulfosalts, identified by WDS electron microprobe, are characterised by a silvery-grey colour in reflected light similar to galena, and display several habits. Sphalerite and Pb-As sulfosalts typically form alternating colloform μm-scale growth bands (Figure 2.8c) in Zones 3 and 4. Grains having a dendritic, sinter-like habit, as described by Hannington (1986), are enclosed in sphalerite in the outer zones of 118693. The dendritic and colloform habits are commonly in close proximity to each other (Figure 2.8d). Parr (1996) identified similar Pb sulfosalts from PACMANUS chimneys as dufrenoysite ($Pb_2As_2S_5$). Irregular blebs form aggregates on sphalerite lining open cavities.

Galena is present in trace amounts in Zones 3 and 4 as anhedral grains intergrown with colloform sphalerite, the individual grains oriented radially outward in the direction of growth (Figure 2.8e). Trace late galena forms as overgrowths on sphalerite and barite in Zones 7 and 8 (Figure 2.8f), typically lining open cavities.

Tabular laths of barite are ubiquitous in Zones 3 to 8. Euhedral grains line open cavities. Amorphous silica forms alternating bands with colloform Zn-sulfides. Anhydrite forms at the transition boundary between Zones 3 and 6. Radiating blades of anhydrite are intergrown with sphalerite and marcasite.

Figure 2.8

(a). Eroded galena crystals enclosed by massive sphalerite. Later-stage euhedral chalcopyrite lines the open conduit. Located Zone 3 (subsample 118693-2), within chimney interior. Reflected plane polarized light . Scale bar = 0.5 μm

(b). Subhedral tennantite overgrowths on sphalerite and chalcopyrite, and protruding into an open cavity. "Wispy" colloform Pb-As sulfosalts are visible within sphalerite. Reflected plane polarized light . Reflected plane polarized light . Scale bar = 100 μm

(c). Pb-As sulfosalt (dufrenoysite?) is intergrown with alternating bands of colloform sphalerite. Reflected plane polarized light. Scale bar = 100 μm.

(d). Dufrenoysite (?) exhibiting both colloform and dendritic textures, intergrown with sphalerite. Reflected plane polarized light. Scale bar = 100 μm

(e). Late galena forms on massive and colloform sphalerite. Pb-As sulfosalts form grains radially parallel with the direction of outward sphalerite growth. Located Zone 3 (subsample 118693-2). Reflected plane polarized light. Scale bar = 0.5 mm

(f). Rounded galena crystals interstitial to (*left*) massive colloform sphalerite-amorphous silica, and (*right*) with barite. Reflected cross polarized light. Scale bar = 0.5 mm

(a)

(b)

(c)

(d)

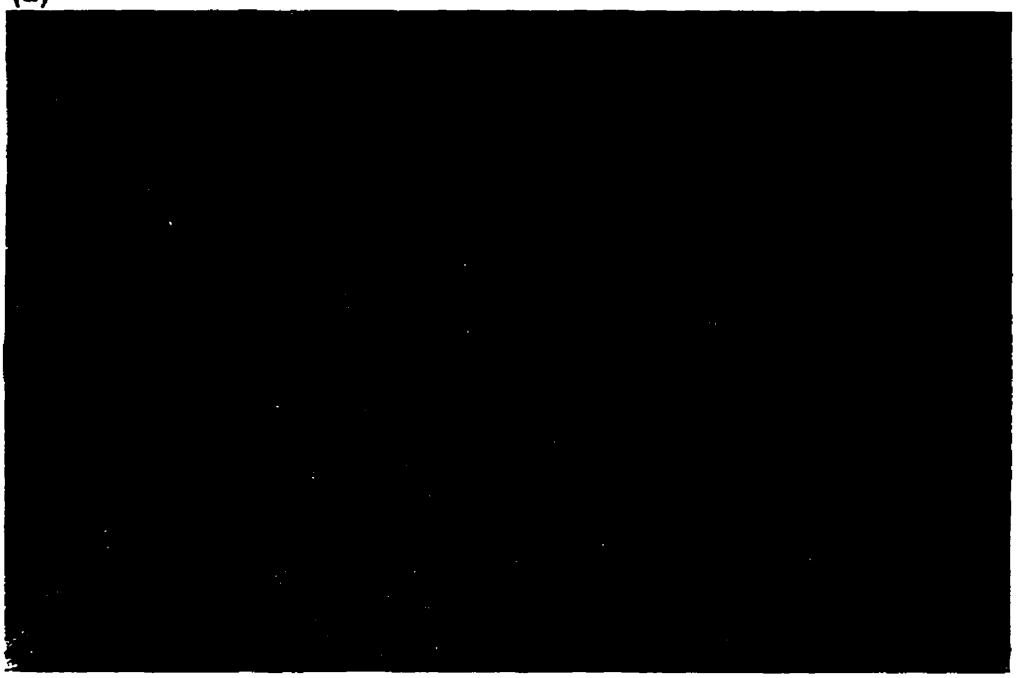

(e)

(f)

Guaymas Basin

Chimneys selected for this study from Guaymas basin are small in size (2-4 cm diameter) and, with one exception are highly friable, due to high carbonate and sulfate content. Chimneys 1966A, 1620 and 1626 are classified as carbonate-sulfate. Chimney 1627 is classified as massive sulfide. Peter and Scott (1988) devised a similar classification, grouping chimneys as "carbonate + sulfate-rich" and "sulfide-rich". The mineralogy of hydrothermal chimneys from Guaymas Basin is described in detail in Peter (1986) and Peter and Scott (1988).

Chimneys classified as carbonate-sulfate are characterised by coarse, intergrown calcite and barite, with minor amounts of finely disseminated sulfides located in the interior walls. Two distinct morphologies of calcite were identified in reflected light. Calcite 1 is characterised by rounded grains forming in aggregates, and displays a characteristically brownish, cloudy colour, likely due to abundant sulfide inclusions (Peter and Scott 1988). Sulfide assemblages are generally associated with calcite 1 aggregates. Calcite 2 is distinguished by larger, euhedral crystals of a cleaner quality. Barite and anhydrite occur as subhedral laths.

Sulfides are typically disseminated within the inner conduit walls. Sphalerite ((Zn,Fe)S) is the dominant sulfide phase. It is intergrown with isocubanite and associated with pyrrhotite and galena. Pyrrhotite ($Fe_{1-x}S$) laths are associated with pyrite, sphalerite and galena. Some pyrrhotite occurs as radial overgrowths on barite and carbonate. Isocubanite ($CuFe_2S_3$) is intergrown with sphalerite, and commonly exhibits chalcopyrite exsolution lamellae.

Galena (PbS) is the only Pb-rich phase at Guaymas Basin, and is found mainly in the inner walls of both high and low temperature sulfate-carbonate chimneys. It forms small irregular grains associated with sphalerite, pyrrhotite, and chalcopyrite bearing isocubanite exsolution lamellae.

Chimney 1627-A3 is a rare example of massive-sulfide at Guaymas Basin. The mineralogy is dominated by sphalerite and Cu-rich phases (chalcopyrite, bornite, idaite), with minor anhydrite and calcite present. No Pb-phases are present.

Figure 2.9

(a). (Chimney 1626-A1, inner wall) Galena intergrown with sphalerite, isocubanite and pyrrhotite. Chalcopyrite exsolution lamellae are visible in isocubanite. Gangue is primarily calcite. Reflected plane polarized light. Scale bar = 100 μm.
(b). (Chimney 1966-A, inner wall) Relict galena and isocubanite replaced (?) by barite. Reflected plane polarized light. Scale bar = 100 μm.

(a)

(b)

BULK GEOCHEMISTRY

Instrumentation and Method

Subsamples from PACMANUS chimney 118693 and all Guaymas Basin chimneys were analysed by instrumental neutron activation analysis (INAA), performed at the University of Toronto. Rock powders weighing 50 mg were sealed into flat plastic baggies in preparation for analysis. Detection of elements at 7 and 40 day counts are summarised in Table 2.4a.

Because hydrothermal Pb forms sulfide, sulfate and carbonate phases, and also occurs as Pb^{++} cations within the barite lattice, complete sample dissolution was necessary for an accurate Pb determination by ICP-AES. Rock powders were treated with concentrated HNO_3-$HClO_4$-HF, followed by a closed-vessel microwave-heated digestion in aqueous Na_2CO_3. This method, developed with the specific intent of attaining complete sample dissolution, is suited to the particular mineralogy of seafloor chimneys.

The analytical method employed in this study is described in detail in Chapter 1. Multi-elemental analyses were carried out at University of Toronto's ANALEST facility, using a Perkin-Elmer Optima 3000DV ICP-AES, equipped with an autosampler. The accompanying Perkin-Elmer ICP WinLab software package, version 1.40, was used to process raw data. Analytical peaks and detection limits for various elements are summarised in Table 2.4b.

A domestic, "kitchen" type General Electric (Model GTC1042W J01) microwave oven, equipped with a rotating stage, was employed for Na_2CO_3 digestions. Variable power output settings allowed power increases in increments of 10%, with a maximum power output of 625 W.

Table 2.4a: Analytical peaks for INAA

Element	Count (days)	Radionuclide	Peak (KeV)
Mo	7	Mo-99	140.3
Ba	7	Ba-131	216.0
Au	7	Au-198	411.8
W	7	W-187	479.5
As	7	As-76	559.1
Sb	7	Sb-122	564.0
Fe	7	Fe-59	1099.3
Na	7	Na-24	1368.7
Hg	40	Hg-203	279.2
Cr	40	Cr-51	320.1
Ag	40	Ag-110	657.6
Ni	40	Ni-58	810.8
Zn	40	Zn-65	1115.5
Co	40	Co-60	1332.5

Table 2.4a: Analytical peaks for ICP-AES

Element	Emission line (nm)	Detection limit (ppm)
Na	330.237	0.031
Mg	280.270	0.002
K	404.721	0.061
K	766.491	0.007
Ca	317.933	0.014
Mn	257.601	0.001
Co	238.892	0.001
Ni	232.003	0.002
Cu	324.754	0.010
Sr	407.771	0.001
Cd	214.438	0.0003
Pb	220.353	0.006
As	193.696	0.011
Fe	238.204	0.001
Ba	233.527	0.001
Sn	189.933	0.002

Results

ICP-AES bulk analyses of hydrothermal chimneys from Eastern Manus Basin, Guaymas Basin, and the southern East Pacific Rise yielded Pb concentrations ranging between 85 ppm and 1.64 wt.%. Subsamples from one PACMANUS chimney were the richest in lead, with concentrations ranging from 0.41 to 1.64 wt.%. A single sulfide-rich chimney from Guaymas Basin, with an average concentration of 95 ppm, was poorest in lead. Lead in Guaymas Basin carbonate-sulfate chimneys ranged from 0.047 to 0.405 wt.%, the higher concentrations representing subsamples from the inner conduit walls. Sulfide chimneys from Pito Deep, southern East Pacific Rise, yielded values averaging 618 ppm.

Lead measurements of several andesites and dacites from the Pacific Antarctic Rise (PAR), ranged from below the detection limit (0.006 ppm) to 1.2 ppm.

Table 2.5: Major and trace element determinations for PACMANUS chimney samples

Sample	118693						132744	132452
Subsample	1	2	3	4	5	6		
Fe_2O_3 %	3.00	1.43	0.83	1.39	0.32	0.15	8.73	1.57
Na	6.49	28.85	31.82	26.49	37.21	37.06	0.50	0.08
Mg	0.01	0.01	0.01	0.01	0.01	0.01	0.83	0.02
K	25.85	16.69	9.13	13.54	3.83	1.29	12.09	1.86
Ca	0.01	0.02	0.03	0.05	0.05	0.06	1.69	23.91
Cu	20.39	9.88	4.40	1.36	1.89	0.55	0.01	0.28
Zn	7.50	30.30	28.36	25.81	32.71	33.30	0.04	0.09
Pb ppm	4053	13438	16433	10758	9362	8470	340	51
Ba	4190	56415	130052	171775	94047	168591	2946	129
Sr	40	806	349	2105	1191	2484	489	2249
As	3589	7795	10532	6134	6695	3350	517	73
Sb	378	1836	2107	1242	2024	1162	108	3
Ni	10	14	13	15	11	13	13	11
Ag	113	261	376	331	299	251	0	5
Co	6	4	3	2	2	1	13	56
Cd	189	873	1044	846	1260	1223	5	3
Mn	35	113	135	238	90	66	1938	22
Mo	18	13	12	27	6	6	nd	nd
Cr	6	0	16	28	0	12	nd	nd
Se	0	1	0	0	0	0	nd	nd
La	0	1	5	5	3	5	nd	nd
W	2	13	13	29	10	43	nd	nd
Ce	0	0	15	3	0	12	nd	nd
Eu	0	1	1	1	0	0	nd	nd
Sc	0	0	0	0	0	0	nd	nd
Au ppb	10182	19440	14321	20007	21965	19653	nd	nd

Determined by ICP-AES: (RSD=3-5%): Na, Mg, K, Ca, Cu, Pb, Sb, Ni, Ag, Cd, Mn; (RSD=6-7%): Sr, As
Fe, Ba, Zn, Mo, Cr, Se, Au, La, W, Ce, Eu, Sc determined by INAA
Fe, Ba, Zn determined by ICP-AES for 132744 and 132452

Table 2.6: Major and trace element determinations for Guaymas Basin chimney samples

Sample	1620-C1		1626-A1		1627-A3			1966-A	
Subsample	1	2	1	2	1	2	3	1	2
Fe_2O_3 %	0.53	0.16	0.46	0.06	3.46	3.72	2.99	0.18	0.03
Na	0.66	0.16	1.29	0.23	26.02	27.95	38.29	0.79	1.14
Mg	0.44	0.10	1.48	1.50	0.36	0.33	1.09	0.01	0.00
K	6.13	1.22	4.01	0.50	39.70	35.88	32.96	1.20	2.08
Ca	36.82	26.90	19.62	27.07	0.41	0.58	0.07	13.91	22.87
Cu	0.18	0.04	2.32	0.23	14.91	13.04	10.33	0.19	0.34
Zn	0.53	0.17	1.52	0.19	24.44	19.22	30.51	0.92	0.12
Pb ppm	4042	865	3979	466	103	99	85	2554	4051
Ba	13684	43271	15259	37314	179	259	174	2537	1703
Sr	3299	4066	3349	6245	28	32	6	2755	4617
As	35	76	132	39	0	0	0	8	22
Sb	55	70	83	20	8	9	4	14	27
Ni	10	7	18	8	15	15	22	5	9
Ag	46	79	90	38	23	19	17	0	56
Co	1	0	1	1	437	395	406	1	1
Cd	26	7	207	35	1659	1829	2211	77	127
Mn	12924	11263	2910	1774	1403	1607	1951	1296	2169
Mo	2	3	1	0	0	0	0	1	4
Cr	8	3	9	6	21	0	12	7	6
Se	14	4	15	2	238	221	183	6	1
La	6	2	17	7	0	0	0	11	1
W	0	6	1	2	0	0	0	0	0
Ce	6	3	23	8	0	0	0	13	2
Eu	1	1	2	1	0	0	0	0	0
Sc	0	0	0	0	0	0	0	0	0
Au ppb	51	45	59	47	45	39	53	22	24

Determined by ICP-AES: (RSD = 3-5%): Mg, Ca, (RSD = 6-7%): Na, K, Cu, Pb, Sr, Ni, Ag, Cd, Mn, (RSD > 15): Co
Na, Mg, K, Ca, Mn, Co, Ni, Cu, Sr, Cd, Pb, As, Sb, Ag determined by ICP-AES
Fe, Ba, Zn, Mo, Cr, Se, Au, La, W, Ce, Eu, Sc determined by INAA

Table 2.7: Major and trace element determinations for all southern East Pacific Rise samples

Sample	7-7	7-10	92ds3-a	92ds3-b	92ds3-c	91ds	91ds1
Fe_2O_3 %	0.00	11.05	4.95	5.10	5.00	4.37	4.80
Na	0.16	15.86	0.13	0.13	0.13	0.22	0.21
Mg	0.02	0.02	1.98	2.00	1.99	1.14	1.18
K	0.00	26.45	7.55	7.93	7.98	7.15	7.19
Ca	0.02	0.03	4.23	4.29	4.30	3.05	3.15
Cu	1.30	0.13	0.00	0.00	0.00	0.00	0.00
Zn	0.18	3.34	nd	nd	nd	nd	nd
Pb ppm	640	596	1	0	0	1	1
Ba	86	195	94	96	90	134	128
Sr	5	11	150	152	149	128	127
As	337	269	nd	nd	nd	nd	nd
Sb	5	33	nd	nd	nd	nd	nd
Ni	6	12	23	22	31	8	8
Ag	nd	nd	nd	nd	nd	nd	nd
Co	26	27	36	36	36	26	28
Cd	36	563	8	8	8	7	7
Mn	7	103	1084	1094	1090	1025	1062
Mo	nd	nd	nd	nd	nd	nd	nd
Cr	nd	nd	nd	nd	nd	nd	nd
Se	nd	nd	nd	nd	nd	nd	nd
La	nd	nd	nd	nd	nd	nd	nd
W	nd	nd	nd	nd	nd	nd	nd
Ce	nd	nd	nd	nd	nd	nd	nd
Eu	nd	nd	nd	nd	nd	nd	nd
Sc	nd	nd	nd	nd	nd	nd	nd
Au ppb	nd	nd	nd	nd	nd	nd	nd

All elements determined by ICP-AES: (RSD=1-3%): Mg, K, Ca, Cu, Ba, As, Ni, Co, Cd, Mn; (RSD=4-5%): Na, Sr; (RSD=9-11%): Pb, Sb

Discussion Of Results

The distribution of Pb, As and Sb across PACMANUS chimney 118693 is shown in Figure 2.10. Concentrations of all three elements are lowest in the chalcopyrite-rich Zone 1 (subsample 1) and in the outer, porous dendritic-sphalerite Zone 8 (subsample 6). High Pb midway between the central conduit and the outer wall suggests precipitation of Pb-As sulfosalts as a result of mixing between vent fluids and ambient seawater. Hannington (1986) postulated that the fine, "sinter-like" texture of such sulfosalts may indicate sudden precipitation from a vent fluids supersaturated in suspended antimonides and arsenides.

By contrast, carbonate-sulfate chimneys from Guaymas Basin show higher Pb in the inner walls (Figure 2.11). Here, galena is associated with pyrrhotite and isocubanite. This assemblage suggests high temperature formation (Hannington et al., 1995). Sulfides are widely and unevenly disseminated throughout 1966A, which may account for the apparent outward increase in Pb concentration across the chimney. Because no mineralogical Pb phases are present in sulfide-rich 1627-A3, it is unclear where its Pb resides.

Figure 2.12 shows that Guaymas Basin chimneys are Pb-rich relative to Cu + Zn (with the exception of the high-temperature Cu-rich 1627-A3). This is expected, given the heavily sedimented nature of the deposit. Continental sediments overlying the Pb-poor (<3 ppm; J. Sinton, University of Hawaii, personal communication, 1994) basalt host rock are a source of lead enrichment. Typical lead concentrations in terrigenous muds and clays range from 20 to 160 ppm (Chester, 1993), their feldspar content acting as a repository for lead. Isotopic studies of Guaymas Basin vent fluids indicate a combined basalt-continental sediment source for lead (Chen et al., 1986; Koski, 1987).

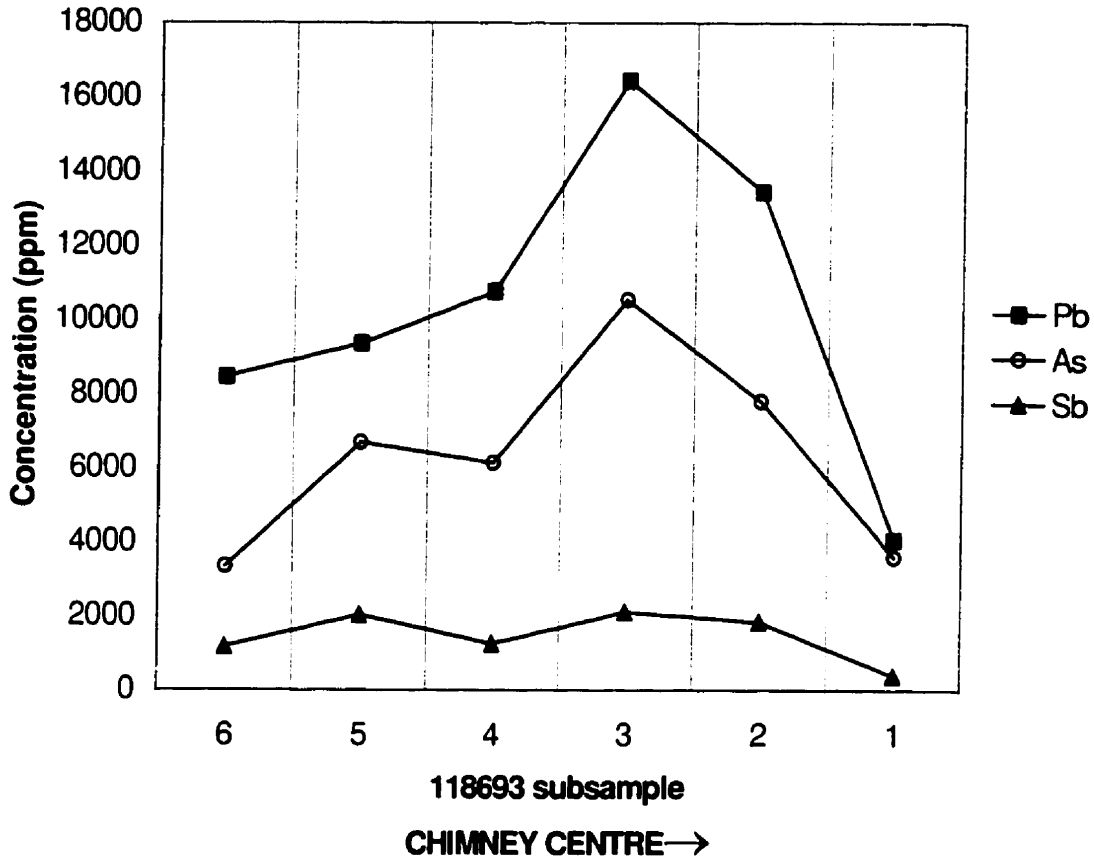

Figure 2.10: Distribution of Pb, As and Sb across PACMANUS chimney 118693

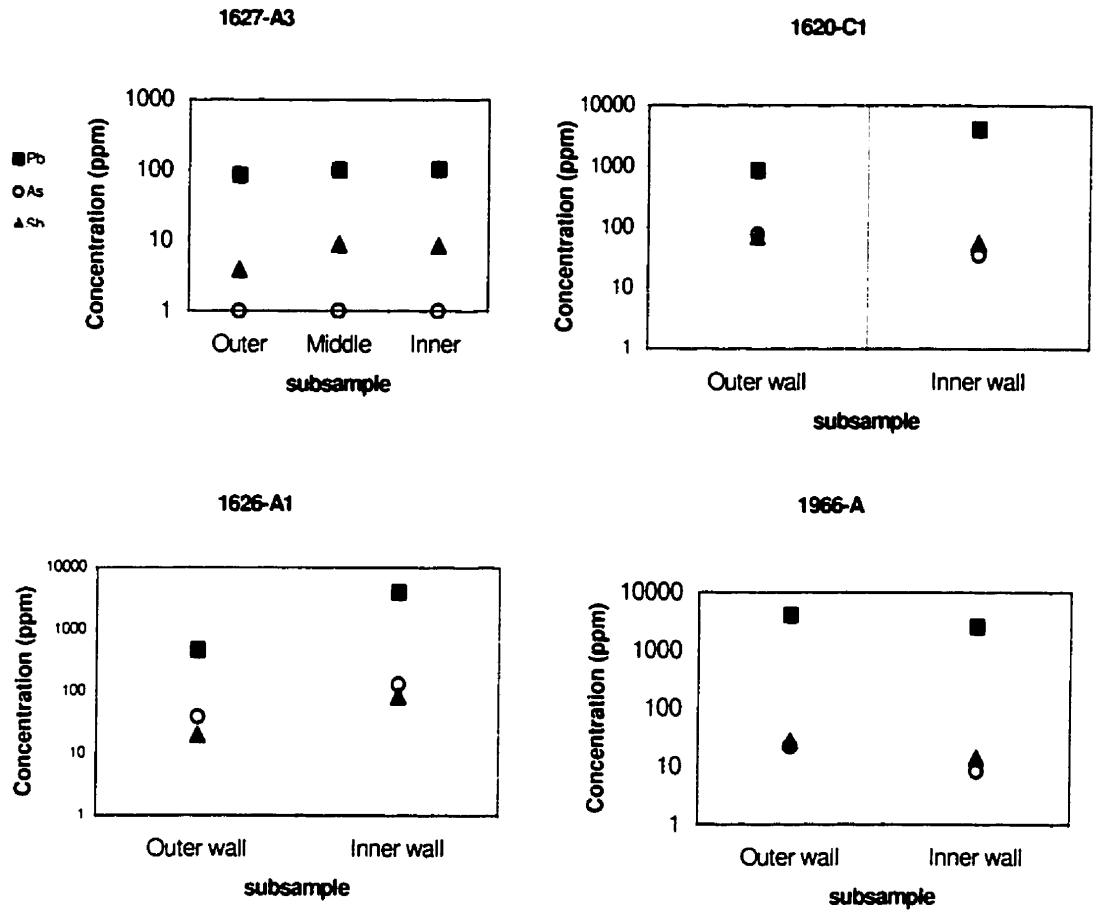

Figure 2.11: Distribution of Pb, As and Sb across all Guaymas chimneys

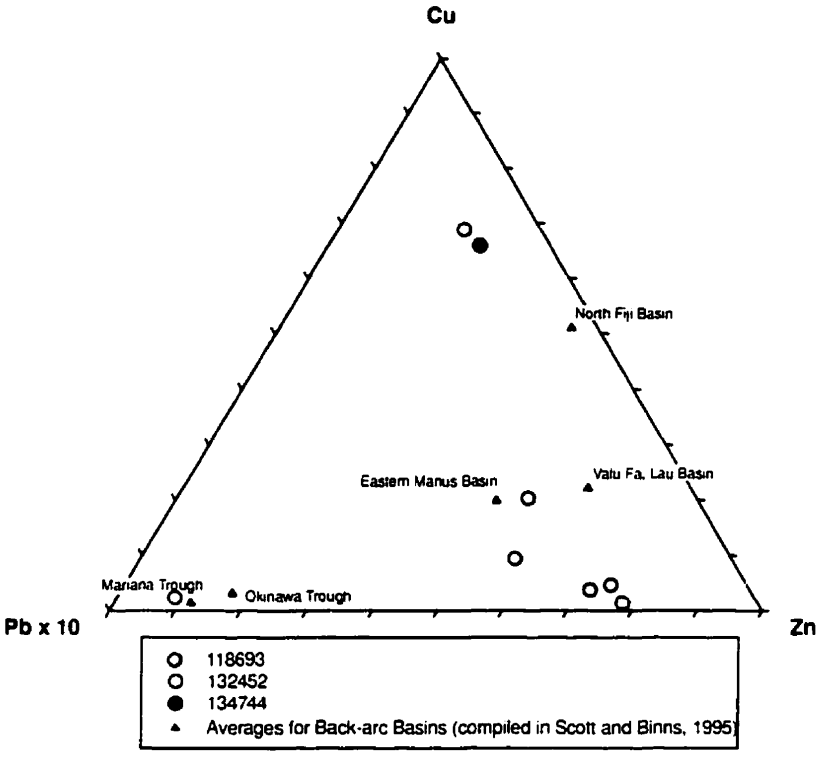

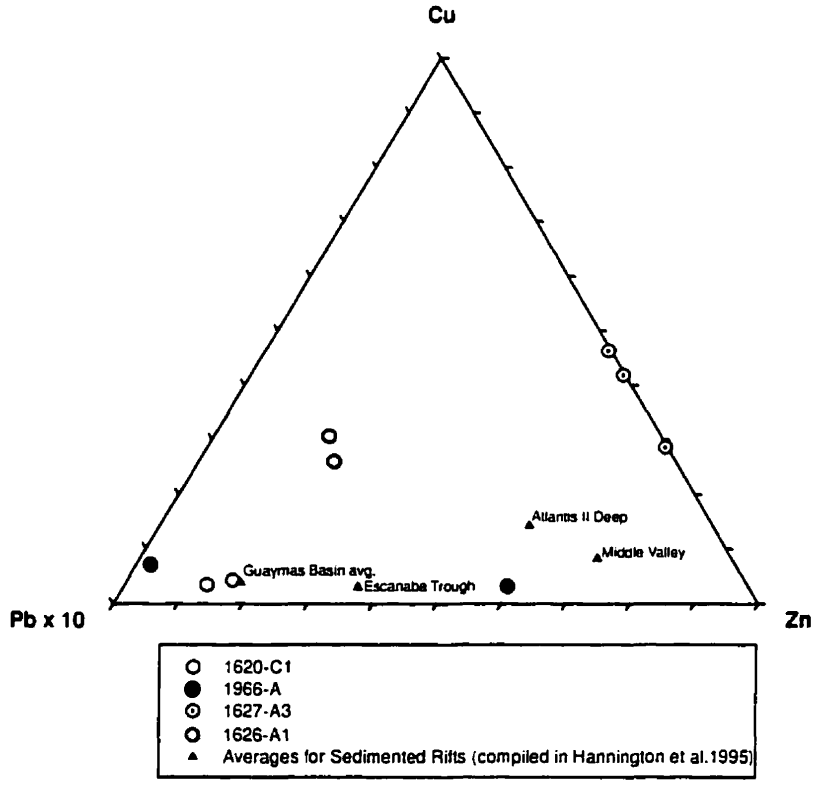

Figure 2.12: Ternary plot showing Zn-Cu-Pb(x10) ratios for subsamples from PACMANUS and Guaymas Basin, in comparison with average values from other deposits from similar tectonic settings.

Cu-Zn-Pb(× 10) ratios for PACMANUS chimneys plot close to the average for eastern Manus Basin (Scott and Binns, 1995) although the Cu/Zn ratios are highly variable across the single chimney 118693. Scott and Binns (1995) showed that Cu-Zn-Pb(× 10) ratios for PACMANUS sulfides reflect the age and tectonic setting of the deposit. They are Pb-rich in comparison to sulfides in mature back-arc basins, such as North Fiji basin, whose Cu-Zn-Pb(× 10) ratios are similar to mid-ocean ridge-hosted systems (Fouquet et al., 1993). However, PACMANUS Pb ratios are lower than those found in young back-arc systems hosted in continental crust, such as the Jade deposit, Okinawa (Fouquet et al., 1993; and Scott and Binns, 1995).

High total Pb in PACMANUS chimneys reflects the felsic composition of the host rock; lead is derived principally from the destruction of feldspars (Hannington et al., 1995). PACMANUS dacite Pb contents range from <5 to 9 ppm (Moss et al, 1997).

Subsamples from sulfide-sulfate chimney 118693 ("Fred") showed positive linear correlation coefficients (95% confidence) with Na, As, Sb, Ag, and Eu (Figure 2.13). The positive correlation between Pb and Ag may be due to high Ag in galena (Moss, 1995) or the presence of a Pb-As-Ag sulfosalt phase. Na, Cr, Co correlate with Pb in carbonate-sulfate chimneys. In contrast, Pb in Guaymas sulfide chimney 1627-A3 showed a strongly negative correlation with Na. The positive correlation of Na with Pb is thought to be an artifact of the Na_2CO_3 digestion of $PbSO_4$. This is supported by its strong negative correlation with Na in subsamples from 1627-A3. Due to its Pb poor nature, no $PbSO_4$ precipitated from this chimney, and therefore the Na_2CO_3 digestion step was not performed.

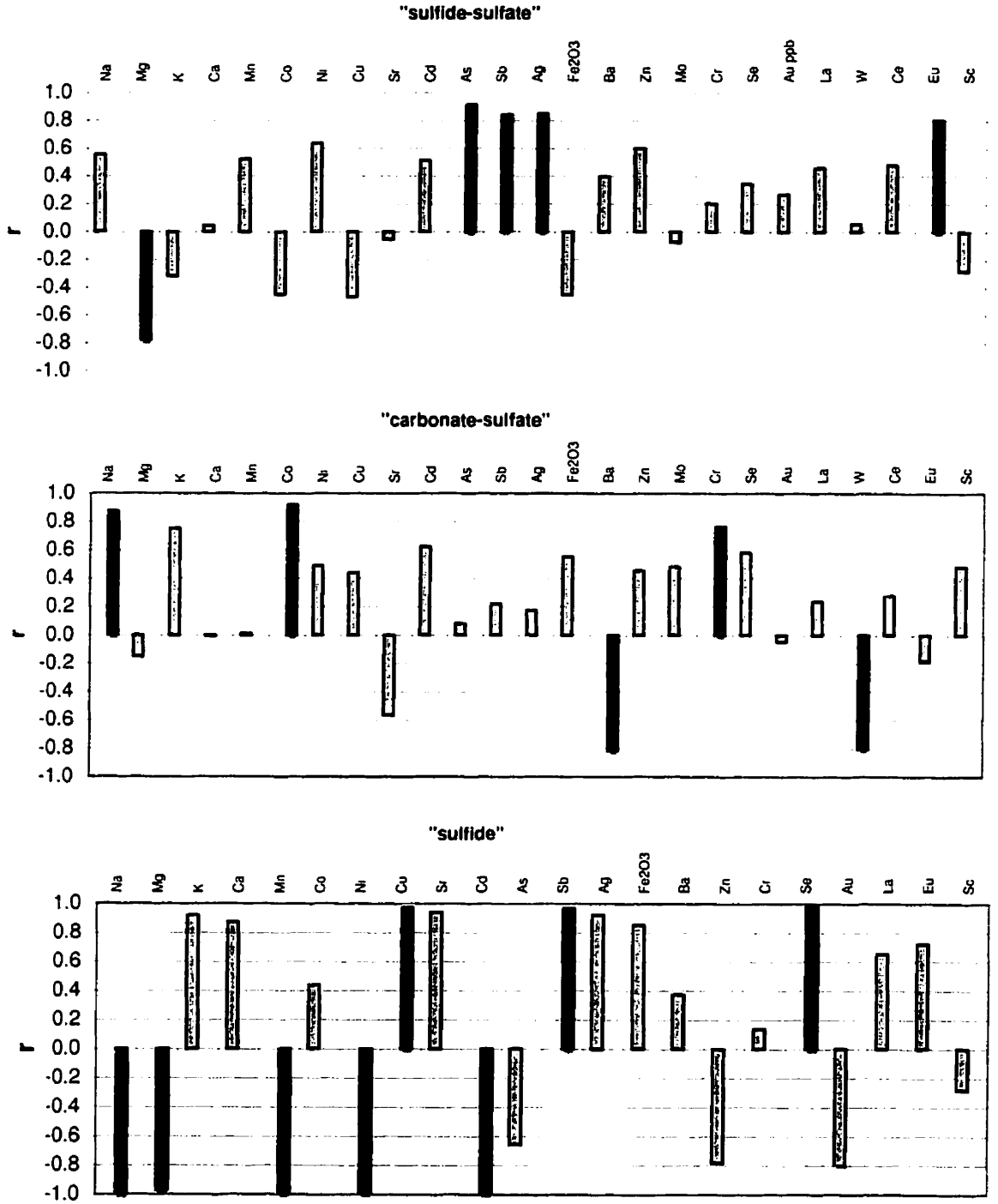

Figure 2.13: Linear correlation coefficients between Pb and other elements from subsamples in a PACMANUS sulfide-sulfate chimney (top), Guaymas Basin carbonate-sulfate chimneys (middle), and Guaymas Basin sulfide chimney (bottom). Black bars indicate a positive or negative correlation at 95% confidence.

CONCLUSIONS

Lead contents in chimneys and mounds from Guaymas Basin, the PACMANUS deposit, and Pito Deep are highly variable, and range from < 100 ppm to 1.6 wt.%. The dominant Pb phase in the PACMANUS sulfide-sulfate assemblage chimney is a Pb-As-(Ag?) sulfosalt, which formed in the middle to outer zones of the chimney. Its coprecipitation with colloform sphalerite and protrusions into open cavities suggest a late, low-temperature formation.

Galena is the only Pb phase in the Guaymas Basin carbonate-sulfate assemblage, and is mainly disseminated in the inner portions of the chimney walls. It is associated with the high temperature chalcopyrite-isocubanite-pyrrhotite assemblage.

Although the absolute abundance of Pb in chimneys from Guaymas Basin is lower than those from PACMANUS, the relative abundance of Pb to Cu + Zn is higher (Figure 2.12). This reflects their contrasting tectonic environments and respective host rocks. The high Pb relative to Cu + Zn in Guaymas Basin chimneys is typical of sedimented hydrothermal deposits (Koski, 1987; and Hannington et al., 1995), and is due to the presence of terrigenous sediments. Cu-Zn-Pb(× 10) ratios for PACMANUS sulfides plot in the middle of the field for deposits in back-arc settings. Total Pb enrichment reflects the abundance of Pb in the host felsic volcanics relative to MORB.

REFERENCES

Binns, R.A. and Scott, S.D. (1993): Actively forming polymetallic sulfide deposits associated with felsic volcanic rocks in the Eastern Manus back-arc basin, Papua New Guinea. Economic Geology (88)8: 2226-2236.

Chen, J.H., Wasserburg, G.J., von Dam, K.L., and Edmond, J.M. (1986): The U-Th-Pb systematics in hot springs on the East Pacific Rise at 21°N and Guaymas Basin. Geochimica et Cosmochimica Acta (50)11, 2467-2479.

Chester, R. (1993): Marine Geochemistry. Chapman & Hall, London.

Constantin, M., Hékinian, R., Bideau, D. and Hébert, R. (1996): Construction of the oceanic lithosphere by magmatic intrusions: Petrological evidence from plutonic rocks formed along the fast-spreading East Pacific Rise. Geology (24)8, 731-734.

Fouquet, Y., von Stackelberg, U., Charlou, J.L., Erzinger, J., Herzig, P.M., Mühe, R., and Wiedicke, M. (1993): Metallogenesis in back-arc environments: The Lau Basin example. Economic Geology (88), 2154-2181.

Hannington, M.D. (1986): Geology, Mineralogy, and Geochemistry of a Silica-Sulfate-Sulfide Deposit, Axial Seamount, N.E. Pacific Ocean. M.Sc. thesis, University of Toronto.

Hannington, M.D., Jonasson, I.R., Herzig, P.M. and Sven, P. (1995): Physical and Chemical Processes of Seafloor Mineralization in Mid-Ocean Ridges. *In*: Seafloor Hydrothermal Systems: Physical, Chemical, Biological, and Geological Interactions. Humphris, S.E., Zierenberg, R.A., Mullineaux, L.S. and Thomson, R.E., ed. Geophysical Monograph 91. American Geophysical Union, 115-157.

Hékinian, R., Stoffers, P., Devey, C., Ackerman, D., Hemond, C., O'Connor, J., Binard, N. and Maia, M. (1997): Intraplate versus ridge volcanism on the Pacific-Antarctic Ridge near 37°S - 111°W. Journal of Geophysical Research – Solid Earth (102), No.B6, 12,265-12,286.

Koski, R.A. (1987): A comparison of sulfide desposits from modern sediment-covered spreading axes with Besshi-type deposits of Japan. *In*: Gorda Ridge: A Seafloor Spreading Center in the United States' Exclusive Economic Zone. McMurray, G.R., ed. Springer-Verlag, 117-130.

Lonsdale, P. (1980): Hydrothermal plumes and baritic sulfide mounds at a Gulf of California spreading center. EOS, Transactions of the American Geophysical Union, 995.

Moss, R. (1995): Distribution of silver in massive sulfide deposits of the East Pacific Rise at 13°N and 21°N. M.Sc. thesis, University of Toronto.

Moss, R., Scott, S.D., and Binns, R.A. (1997): Concentrations of gold and other ore metals in volcanics hosting the Pacmanus seafloor sulfide deposit. JAMSTEC Journal of Deep Sea Research, (13), 257-267.

Parr, J.M., Binns, R.A. and Gemmell, J.B. (1996): Sulfide chimneys from the Satanic Mills site in the PACMANUS hydrothermal field, eastern Manus Basin, Papua New Guinea. EOS, Transactions, American Geophysical Union, May 28, 1996; Vol. 77(22), p.W120

Parr, J.M., Murao, S.M. and Binns, R.A. (1995): A comparison of massive sulfides deposits forming at the PACMANUS (Manus Basin, PNG) and JADE (Okinawa Trough, South China Sea) seafloor hydrothermal fields. Proceedings of the 1995 PACRIM Congress. J.L. Mauk and J.D. St.George, eds. Australasian Institute of Mining and Metallurgy.

Peter, J.M. (1986): Genesis of Hydrothermal Vent Deposits in the Southern Trough of Guaymas Basin, Gulf of California: A Mineralogical and Geochemical Study. M.Sc. thesis, University of Toronto.

Peter, J.M., Peltonen, P., Scott, S.D., Simoneit, B.R.T., and Kawka, O.E. (1991): ^{14}C ages of hydrothermal petroleum and carbonate in Guaymas Basin, Gulf of California: Implications for oil generation, expulsion, and migration. Geology (19), 253-256.

Peter, J.M. and Scott, S.D. (1988): Mineralogy, composition, and fluid-inclusion microthermometry of seafloor hydrothermal deposits in the southern trough of Guaymas Basin, Gulf of California. Canadian Mineralogist (26): 567-587.

Peter, J.M. and Shanks III, W.C. (1992): Sulfur, carbon and oxygen isotope variations in submarine hydrothermal deposits of Guaymas Basin, Gulf of California. Geochimica et Cosmochimica Acta 56, 2025-2040.

Peucker-Ehrenbrink, B., Hofmann, A.W., and Hart, S.R. (1994): Hydrothermal lead transfer from mantle to continental crust: the role of metalliferous sediments. Earth and Planetary Science Letters 125, pp.129-142.

Rona, P.A. and Scott, S.D. (1993): Preface In: A special issue on sea-floor hydrothermal mineralization: New perspectives. Economic Geology (88)8: 1935-1976.

Scott, S.D. and Binns, R.A. (1995): Hydrothermal processes and contrasting styles of mineralization in the western Woodlark and eastern Manus basins of the western Pacific. In: Parson, L.M., Walker, C.L. and Dixon, D.R. (eds), 1995, Hydrothermal Vents and Processes. Geological Society Special Publication No. 87, 191-205.

APPENDIX 1

Power calibration of a domestic microwave oven

I. Calibration Procedure (after EPA Method 3051)

Equipment

- deionized H_2O
- Nalgene PP beakers, with a capacity of 800 g
- top-loading electronic balance, accuracy ± 0.1 g
- domestic General Electric (Model GTC1042W J01) microwave oven, equipped with a rotating stage
- mixer and magnetic stirring bars
- glass-bulb thermometer, with gradations to 0.2°C

Procedure

1] Weigh 800 g ± 0.1 g deionized H_2O into a Nalgene beaker
2] Allow the water to equilibrate to room temperature, in the range 22 ± 2°C. Record the water temperature
3] Heat the beaker in the microwave for 2 minutes at power settings increasing in 10% increments from 10 to 100%
4] Remove the beaker from the oven and stir vigorously for 20 seconds
5] Record the maximum temperature
6] The water can be reused for further measurements when it has returned to room temperature.

II. Calculation of absorbed power

Absorbed power is calculated using the following equation,

$$P = \frac{KC_p M\Delta T}{t}$$

where P is the absorbed power expressed in watts; the constant K (4.184) converts calories to watts; C_p is the heat capacity in cal/(g·°C); M is mass of H_2O; ΔT is the increase in temperature after heating (final temperature minus initial temperature); and t represents time in seconds.

APPENDIX 2

Method for Acid and Na_2CO_3 Digestion of Rock Samples in Preparation for Pb Determination by ICP-AES

Reagents

deionized water
69% HNO_3 (w/w), 15.4M
10% HNO_3
48% HF (w/w), 29M
60% $HclO_4$ (w/w), 6.9M
Na_2CO_3 reagent powder
500 ppm Ba standard

Equipment

alumina mill
agate mortar and pestle
balance, reproducibility ± 0.001 g
hot plate
ultrasonic bath
centrifuge
shaker
60 ml Teflon screw-cap vessels
50 ml centrifuge tubes, labelled #1 and #2.
tube rack
100 and 25 ml volumetric flasks
1 ml, 5 ml and 10 ml pipettes
125 ml polypropylene bottles
microwave oven, 500W, variable power output, equipped with rotating stage

Procedure

I. DIGESTION OF SULFIDES, CARBONATES, ORGANIC MATTER

1] Rock is crushed to 2 mm chips and ground using alumina mill, or a mortar & pestle if material is very friable.
2] 0.5 ± 0.001 g sample is weighed into 60 ml Teflon screw-cap vessels.
3] Approximately 2 ml deionized water is added to wet sample.
4] Add 10 ml concentrated HNO_3 and place closed vessel in ultrasonic bath for 5 minutes. Uncap vessel and evaporate solution to near dryness on hot plate at 150°C.
5] Add 10 ml concentrated HNO_3 and heat until about ¾ of solution has evaporated. Dilute with 15 ml water.
6] Place capped vessel in ultrasonic bath for 5 minutes. Return to hot plate and heat for 15 minutes, swirling solution.
7] Transfer solution, undissolvable solids, and rinse water to 50 ml centrifuge tube #1. Centrifuge at high speed for 15 minutes.

8] Decant off solution to 50 ml centrifuge tube #2. Set aside tube #2. If any solids were accidentally transferred to tube #2, remove to tube #1 with a pipette.

II. DIGESTION & DISSOLUTION OF OXIDES AND SILICATES

9] Add 10 ml HF tube #1 in aliquots. The capped tube may be placed in an ultrasonic bath for 1 minute to loosen material adhering to the sides of the tube. Transfer HF and solids back to Teflon vessels. Add 3 ml $HClO_4$ to Teflon vessel. Tube #1 should be thoroughly rinsed clean with water.

10] Heat capped Teflon vessels 3-4 hours, on hot plate at 150°C.

11] Remove vessels from heat and allow to cool. Tap lids to shake condensation from surface. Remove lids and allow the HF-$HClO_4$ solution to completely evaporate at 100-150°C.

12] Add 10 ml dilute HNO_3 and warm for 15 minutes, swirling to dissolve solids.

13] Transfer solution and any undissolvable solids back to tube #1. Centrifuge at high speed for 15 minutes.

14] Decant off solution to tube #2. Using a shaker and centrifuge, rinse solids twice with deionized water, adding rinse water to tube #2.

15] Transfer solution in tube #2 to a 100 ml volumetric flask and dilute to volume. Transfer to 125 ml polypropylene bottles for ICP analysis. This is solution "b".

III. DIGESTION AND DISSOLUTION OF SULFATES

16] Weigh clean Teflon vessel. Transfer undissolved sulfate solids from tube #1 to Teflon vessel. Heat solids to dryness and weigh by difference.

17] Prepare a batch of Na_2CO_3 solution in the proportion 1 g Na_2CO_3 powder to 10 ml deionized water. The ultrasonic bath will increase the carbonate dissolution rate.

18] Add to the Teflon vessel sufficient Na_2CO_3 solution to satisfy a 1:10 sulfate to carbonate weight ratio.

19] Cap vessel tightly and microwave at 100% power for 3 minutes.

20] Lower to 30% power for 10 minutes.

21] Place in ultrasonic bath for 5 minutes.

digestion batches 1,2,3	digestion batches 4,5
22] Repeat steps 28-30.	22] Allow to cool and uncap. Take up solution and solids with a 50 ml syringe and filter through nitro-cellulose filter paper.
23] Allow to cool, uncap, and transfer solution and solids to clean 50 ml centrifuge tube. Centrifuge for 20 minutes at high speed.	23] Rinse solids on filter with deionized water. Test for SO_4^{-2} by adding several drops of 500 ppm Ba standard to rinse water. If $BaSO_4$ precipitates, continue rinsing and retest until no sulfate precipitation is observed.

24] Decant and discard the solution. Rinse and centrifuge solids at least twice more. Test for SO_4^{-2} by adding several drops of 500 ppm Ba standard to rinse water. If barite precipitates, continue rinsing and retest until no barite precipitation is observed.

25] Add 10 ml dilute HNO_3 to centrifuge tube. The solids should effervesce as they dissolve. If any solids remain, centrifuge and decant off the solution to a second tube. The solids must then be retreated according to steps 21-26.

26] Transfer solution to a 25 ml volumetric flask and dilute to volume. Keep solution in 125 ml PP bottles for ICP analysis. This is the "g" solution.

24] Add 10 ml dilute HNO_3 filter. The solids should effervesce as they dissolve off the filter. Conserve dissolved solution.

25] Transfer solution to a 25 ml volumetric flask and dilute to volume. Keep solution in 125 ml PP bottles for ICP analysis. This is the "g" solution.

APPENDIX 3

Chemical constants

Reagent	Molecular Wt. (g/mol)	Concentration (w/w)	Molarity	Density (g/ml)
HNO_3	63.012	69%	15.4	1.41[1]
		27-36%	6.0	
HF	20.006	50%	29.0	1.16[2]
$HClO_4$	100.457	60%	6.9	1.54[2]

[1] from Weast and Astle (1983)
[2] from Harris (1991)

APPENDIX 4

Chemical reactions in acid and Na_2CO_3 digestions

Moderate HNO_3 addition:

(1)* $PbS_{(s)} + 4\ HNO_{3(aq)} \Rightarrow Pb(NO_3)_{2(aq)} + 2\ NO_{2(g)} + 2H_2O_{(l)} + S_{(s)}$

(2)* $S_{(s)} + 6HNO_{3(aq)} \Rightarrow H_2SO_{4(aq)} + 6\ NO_{2(g)} + 2\ H_2O_{(l)}$

Concentrated HNO_3 addition:

(3)* $PbS_{(s)} + 8HNO_{3(aq)} \Rightarrow PbSO_{4(s)} + + 8NO_{2(g)} + 4H_2O_{(l)}$

Digestion of $PbSO_4$ by Na_2CO_3 solution, followed by liberation of Pb by HNO_3 addition

(1) $2Na_2CO_{3(s)} + 2H_2O + 3PbSO_{4(s)} \Rightarrow 2Na_2SO_{4(aq)} + Pb_3(CO_3)_2(OH)_{2(s)} + H_2SO_4$

(2) $6HNO_3 + Pb_3(CO_3)_2(OH)_{2(s)} \Rightarrow 3Pb(NO_3)_2 + 4H_2O + 2CO_2\ (g)$

*from Taylor (1956)

APPENDIX 5

Investigations Into The Effectiveness Of $PbSO_4$ + $BaSO_4$ Digestions By Microwave-Heated Na_2CO_3 Solution

Summary

Experiments were carried out to determine whether the furnace-heated, closed-vessel aqueous Na_2CO_3 digestion method described by Parisot (1997) and Breit et al. (1985) is

1) effective as microwave-driven process with faster reaction rate, and;
2) able to digest both $PbSO_4$ and $BaSO_4$.

Several concentrations of aqueous Na_2CO_3 were tested in the interests of optimising the reaction rate.

Experimental method

Reagents

Fisher reagent $BaSO_4$ powder
Fisher reagent $PbSO_4$ powder
Na_2CO_3 powder
10% HNO_3
Fisher 1000 ppm Pb AA standard
ultrapure deionised water
Mettler balance

Equipment

ultrasonic bath
centrifuge
60 ml Teflon screw-cap vessels
50 ml centrifuge tubes
General Electric (Model GTC1042W J01) "kitchen"-type microwave oven; maximum power output of 625 W; equipped with a rotating stage and variable power output settings, with power increases in increments of 10%
Perkin-Elmer 4000 Atomic Absorption Spectrophotometer, with an air acetylene flame

Procedure

Two variables - $PbSO_4$ weight and the Na_2CO_3 dilution factor - were introduced. The microwave heating routine and the 1:10 ratio of sulfate to Na_2CO_3 (Parisot 1997. and Breit et al. 1985) were kept constant.

Twelve samples of approximately 100 mg $BaSO_4$ powder were weighed by difference and placed in 60 ml Teflon vessels. Weights of 0 (blank), 1 or 2 mg $PbSO_4$ were added, so that total sample weights ($BaSO_4$ + $PbSO_4$) ranged from 99.9 mg to 105.6 mg (Table 1).

125 ml of 1:10 Na_2CO_3 solution (0.94M) was prepared by dissolving 12.5 g Na_2CO_3 powder in a beaker containing 125 ml deionised H_2O. A 1:20 Na_2CO_3 (0.47M) solution was prepared by dissolving 12.5 g Na_2CO_3 in 250 ml deionised water. Carbonate dissolution time was shortened by placing the beakers in a heated ultrasonic bath.

The experimental set-up allowed 2 samples for each combination of $PbSO_4$ weight and Na_2CO_3 dilution (Table 2). All vials contained roughly 100 mg total sulfate weight and therefore required 100 mg × 10 = 1 g Na_2CO_3 for complete decomposition. Therefore those samples slated for the 1:10 Na_2CO_3 solution received 10 ml of solution total; and those slated for the 1:20 Na_2CO_3 solution received 20 ml of solution. Vials 4 and 8 were treated with plain deionized H_2O as a control.

All twelve PFTE vessels were tightly capped and subjected to the microwave heating routine used in this study. The solids were then rinsed and treated with 10% HNO_3.

A 20 ppm lead standard was prepared from a 1000 ppm AA standard in 10% HNO_3. All sample solutions were diluted 100X with 10% HNO_3, up to a volume of 100 ml. A blank of pure deionized water proved more reliable than the $BaSO_4$ blank.

Boiling and minor leakage was observed in some vessels during heating.

Pb was detected using the peak at 283.3 nm.

TABLE A-1: Experimental set-up for $PbSO_4$ + $BaSO_4$ digestions by microwave-heated Na_2CO_3 solutions

Reaction vessel	$BaSO_4$ (mg)	$PbSO_4$ (mg)	Na_2CO_3:H_2O
1	99.9	0	1:10
2	102.4	0	1:10
3	100.2	0	1:20
4	102.1	0	H_2O blank*
5	99.9	1.1	1:10
6	100.5	1.2	1:10
7	103.3	1.1	1:20
8	101.4	1.0	H_2O blank*
9	101.8	2.0	1:10
10	101.4	2.1	1:10
11	103.0	2.0	1:20
12	103.5	2.1	1:20

*H_2O added in place of Na_2CO_3 solution

Results and Discussion

The results indicate that the microwave method provided sufficient heat to digest mixtures of $BaSO_4$ + $PbSO_4$, using a 1:10 ratio of sulfate to Na_2CO_3 (Table A-2). Samples with sulfate masses exceeding approximately 150 mg required extended heating times, in order to allow the resulting larger volumes of solution (>30 ml) to reach the same temperature. However, this was not common, since 150 mg is 30% of 500 mg, and barite content in natural hydrothermal systems rarely exceeds 30% by weight.

Greater dilutions of Na_2CO_3 solutions are more efficient for sulfate digestion. Samples treated with Na_2CO_3 solutions at a 1:20 dilution (0.47M) yielded higher Pb recoveries than those treated with the 1:10 (0.94M) Na_2CO_3 solution. Earlier tests using a 1:5 dilution ratio failed to digest most material. Earlier work (Breit et al. 1985 and Parisot 1997) indicates that the 1:10 dilution is also effective, but at the cost of much longer heating times (Table A-3)

TABLE A-2: Results for $PbSO_4$ + $BaSO_4$ digestions by microwave-heated solutions

Digestion vessel	Measured Pb (μg)	Background Corrected Pb* (μg)	Expected Pb (μg)	Total Pb loss (μg)	Total Pb loss (%)
2	12	0	0	-	n/a
3	16	0	0	-	n/a
5	1177	1163	751.5	-412	n/a
6	425	411	819.8	409	50
7	725	711	751.5	41	5
9	310	296	1366.4	1070	78
10	641	627	1434.7	807	56
11	1131	1117	1366.4	249	18
12	1250	1236	1434.7	199	14

NOTES:

1) Total Pb background corrected by subtracting the averaged background Pb count (14 μg).
2) Results not listed for digestion vessels 1, 4, and 8, which were blanks.
3) Possible contamination in vessel 5.
4) Poor lead recoveries attributed to incomplete digestion in samples treated with 1:10 Na_2CO_3 solution (i.e., vessels 2, 5, 6, 9, and 10).

TABLE A-3: Na_2CO_3 dilutions and heating times

Reference	Dilution (Na_2CO_3:water)	Heat Source	Temperature	Heating Time
Parisot (1997)	1:10	Furnace	95°C	1.5 days
Breit et al. (1985)	1:20	Furnace	95°C	4 hours
This study	1:20	Microwave oven	Not quantified	30 minutes

APPENDIX 6

Evaluation of Pb recovery in GUA, PAC, and MP-1a replicates, with respect to $Na_2CO_{3(aq)}$ digestion

Standard	Na	Pb		Measured 'b'	Measured 'g'	Expected in 'g'[b]	Measured 'g' / Expected in 'g'	Total Recovery	Total liquid load in microwave run
	Measured 'b'	Expected Total							
	(ug)	(ppm)	(ug)[a]	(ug)	(ug)	(ug)		(%)	(ml)
GUA-1	2.65	433	211	144	21	67	0.3133	78.3	155
GUA-2	2.69	433	223	143	24	79	0.3030	75.2	155
GUA-3	5.57	433	252	159	24	93	0.2571	72.6	155
GUA-4	0.02	433	219	149	10	70	0.1475	72.9	250
PAC-1	12.42	25980	13156	6973	4101	6183	0.6632	84.2	155
PAC-4	6.63	25980	12525	8434	2154	4091	0.5265	84.5	250
PAC-5	4.99	25980	13055	10602	1659	2453	0.6766	93.9	250
MP-1a-2	1.56	43300	8699	8530	4	169	0.0210	98.1	155
MP-1a-3	7.55	43300	8716	8636	1	81	0.0104	99.1	155
MP-1a-4	0.02	43300	9881	9595	7	286	0.0246	97.2	250
kc-1	5.10	68700	18109	16536.56	6.53	1573	0.0042	91.4	250

[a] equivalent total μg Pb, calculated as (ppm Pb) x (total sample weight in grams)

[b] calculated as (Expected Total) - (Measured 'b'). This assumes negligible Pb loss by volatilisation or other routes